ISSN 1349-1113
JAXA-RR-04-014E

JAXA Research and Development Report

Numerical Study on the Lateral Jet Flow of Helicopter Rotor: Part 2. Blade Vortex Interaction Noise of Rotary Wing

Choongmo YANG, Takashi AOYAMA,
Shigeru SAITO and Jehyun BAEK

January 2005

Japan Aerospace Exploration Agency

CONTENTS

Numerical Study on the Lateral Jet Flow of Helicopter Rotor: Part 2. Blade Vortex Interaction Noise of Rotary Wing*

Choongmo YANG*[1], Takashi AOYAMA*[1], Shigeru SAITO*[1], and Jehyun BAEK*[2]

ヘリコプタロータの翼端噴射に関する数値解析：第2部　回転翼のブレード／渦干渉騒音

梁忠模*[1]、青山剛史*[1]、齊藤茂*[1]、Jehyun BAEK*[2]

ABSTRACT

Blade vortex interaction (BVI) noise, which is generated by impulsive changea in the pressure over the interacting blade preceding the pressure jump, propagates sound to far field observers. In general, these interactions occur in forward-descent flight conditions, especially during a landing approach. The acoustic signal from BVI is generally in the frequency range to which the human subjective response is most sensitive. In order to reduce BVI noise, many researchers have been studying not only passive remedies such as rotor tip design and leading edge modification, but also active devices such as the higher harmonic control method, active tab, active flap, and tip-jet blowing.

The National Aerospace Laboratory (NAL) in Japan and Pohang University of Science and Technology (POSTECH) in Korea have conducted a collaborative research program on the effects of lateral wing-tip blowing to reduce BVI noise from helicopter rotors. The lateral wing-tip method is one of the active control methods to control the generation and behavior of tip vortical flow by blowing a jet flow at the tip of the main rotor. In the first stage of the research, three-dimensional compressible Euler/Navier-Stokes equations are solved to calculate the effect of blowing air from the blade tip on the tip vortex of a fixed single blade. In the next stage, predictions of BVI noise will be made by combining an unsteady Euler code with an aeroacoustic code based on the Ffowcs-Williams and Hawkings formulation.

In the present report, predictions of BVI noise are performed for a two-blade rotor. A moving overlapped grid system with three types of grids including blade, inner and outer background grids is used to simulate the BVI of a helicopter with two blades in forward/ descending flight. The body-fitted blade grid moves with the blade motion, and the background grids in this Cartesian system are placed around the rotor disk in order to include the trace of the tip vortex. The effects of lateral blowing in the tip region to reduce BVI noise are examined using various jet blowing conditions including jet speed, jet slit area and injection direction, which are also used in the fixed rotor calculations. Calculations show that the reductions in BVI noise peak and the sound pressure level are more dependent on the jet velocity and flow rate than on jet directions, and the maximum decrease in BVI noise is 2.55 dB.

Keywords: Blade Vortex Interaction (BVI), CFD, Euler Equation, Helicopter, Tip vortex, Aeroacoustics, Ffowcs-Williams and Hawkings formulation, Overlapped Grid

概　　要

ブレード／渦干渉（Blade-Vortex Interaction: BVI）騒音は、先行するメイン・ロータのブレードが吐き出した翼端渦が後続ブレードの翼端付近を通過する時に起こる弱い干渉、あるいは先行ブレードの翼端渦を後続ブレードが切る時に起こる強い干渉によって、ブレードの空力荷重が急激に変動することから発生する。この騒音は、特に前進方向の下方に指向性を持ち、主にヘリコプタが着陸する際に発生するため、付近の住民に与える影響が大きく、都市部に

* Received 26 August, 2004

*1 Japan Aerospace Exploration Agency (JAXA), JAPAN

*2 Pohang University of Science and Technology (POSTECH), KOREA

おけるヘリポート設置の妨げとなっている。BVI騒音の低減法としては、翼型や翼端形状を工夫する受動的なものから、高調波制御、アクティブ・フラップ、翼端噴射などの能動的なものまで、様々な方法が提案されている。

航空宇宙技術研究所（NAL）と韓国の浦項工科大学校（POSTECH）は、能動的なBVI騒音低減法の中で、特に翼端噴射に着目して、その低減効果をCFDで解析することを目的に、共同研究を行った。この翼端噴射とは、ヘリコプタ・ブレードの翼端から半径方向外向きにジェットを噴き出すことで、翼端渦の位置や構造を変化（渦の循環を弱めたりコア半径を大きくする）させ、BVI騒音を低減しようとする技術である。本研究では、まず、単一格子を用いて固定ブレードの翼端噴射が翼端渦の挙動に及ぼす影響をEuler/Navier-Stokesコードで解析した。続いて、移動重合格子法を用いた3次元非定常Eulerコードと Ffowcs Williams and Hawkings（FW-H）の式に基づく空力音響コードを組み合わせた計算法によって、回転場での翼端噴射の騒音低減効果を解析した。

本報告は、後者の回転場での解析結果について述べるものである。ここで用いた方法が、実験値との比較を通して、BVI騒音の特徴であるピーキーな音圧波形をよく予測することが示されたので、翼端噴射のBVI騒音低減効果を解析する方法として適切であることが確認された。移動重合格子法の計算に用いた格子は3種類（ブレード格子、内側背景格子、外側背景格子）である。ブレード格子は、ブレード1本の周りを覆い、ブレードと共に回転運動を行う物体適合格子であり、背景格子はブレードから放出された翼端渦を捉えるための直交格子である。ここでも、固定ブレードの計算で検討した翼端噴射速度、噴射方向、噴射口面積をパラメトリックに変化させて翼端渦の挙動に及ぼす影響を解析した。結果として、翼端噴射では、噴射方向が騒音に及ぼす影響は小さく、噴射量と噴射速度を大きくすることが騒音低減に有効であり、最大2.55dBの低減効果が確認できた。

1. INTRODUCTION

1.1 BVI in helicopter

There are several kinds of noise sources in helicopter as shown in Figure 1.1. Among these noises, rotor noises including main rotor and tail rotor, are of interest in the fields of aerodynamics and aeroacoustics. The mechanism of BVI noise generation is impulsive change in the pressure distribution over the interacting blade preceding pressure jump, as shown in Figure 1.2[1]. These sudden changes in pressure propagate sound to far field observer. In general, the interactions occur in descent flight conditions, especially during approach to a landing. The noise generated by the interactions radiates mostly below the helicopter's tip-path plane in the direction of forward flight. The acoustic signal is generally in the frequency range most sensitive to human subjective response (500 to 5000Hz)[2, 3]. The BVI noise, therefore, prevents that the commuter helicopter is widely used in the densely populated area.

The blade vortex interaction can be viewed as an unsteady, three-dimensional close encounter of a curved-line vortex, at an arbitrary intersection angle, as shown in Figure 1.3(a)[4] The limiting cases of such encounter for $\Lambda = 0o$ and $90o$ are drawn in Figure 1.3(b) and (c), which are corresponding to the parallel blade vortex interaction and vertical blade vortex interaction,

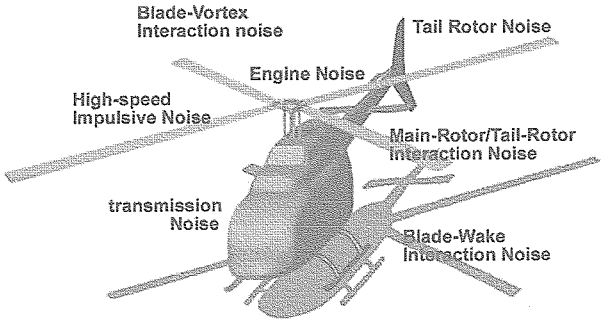

Figure 1.1 Several noises in helicopter

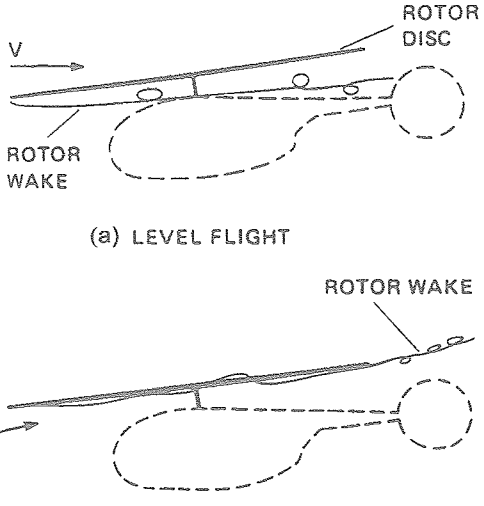

Figure 1.2 Interaction of tip vortices with a rotor disk for level and descending flight

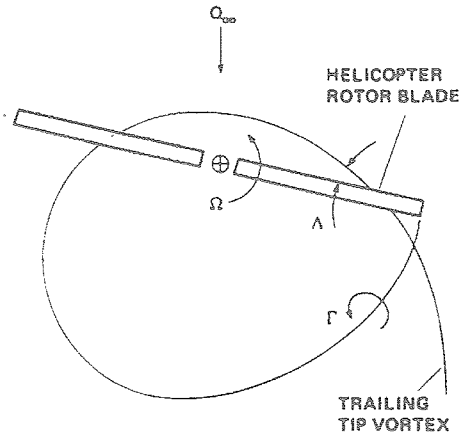

(a) Diagram of BVI

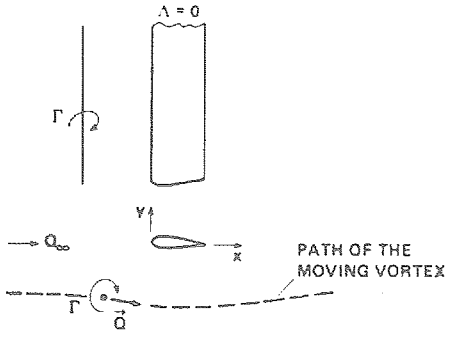

(b) parallel blade vortex interaction

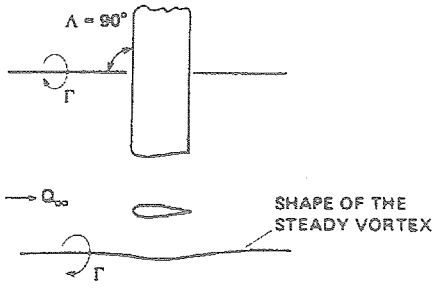

(c) vertical blade vortex interaction

Figure 1.3 Diagram and two critical cases of BVI

respectively. The former encounter is essentially two-dimensional but unsteady, whereas the latter can be considered as steady but highly three-dimensional.

Figure 1.4[5] show an example of a typical wave form of full-scale in-flight helicopter impulsive noise including high speed compressibility noise and blade vortex interaction noise. The series of positive and negative peak values are associated with blade vortex interactions, and the following large negative peak comes from high-speed noise. All of these impulsive features originates from rapid pressure changes, and it may cause weak shock wave. Thus both high-speed noise and blade vortex interaction noise are complicated phenomena of nonlinear, or transonic effects in the flow field around the blade and in the resulting radiating wave.

At low speed, the rotor wake stays in the hover plane for several rotor revolutions during the interactions because of positive inflow conditions, resulting in complicate aerodynamic and structural dynamic problems. During these interactions, the tip vortex may be distorted and enlarged because it is close to blade. The tip vortex will affect the blade flapping, torsional deformations and these blade deformations will in turn modify the wake structures. Computational modeling of these phenomena may require a reliable, comprehensive analysis and particularly wake modeling with high order accuracy such as vortex-embedding technique, or adaptive unstructured-grid system in order to prevent numerical dissipation[6].

1.2 Various methods to reduce helicopter rotor noise

The aerodynamics and acoustics of BVI have been examined both analytically and experimentally up to now, and many researches have been conducted to reduce or control BVI noise[7–10]. Several methods which couple aerodynamic and aeroacoustic codes have been developed to predict the BVI noise by the Aero-Flight-dynamics Directorate (AFDD) of the U.S.Army[11], DLR

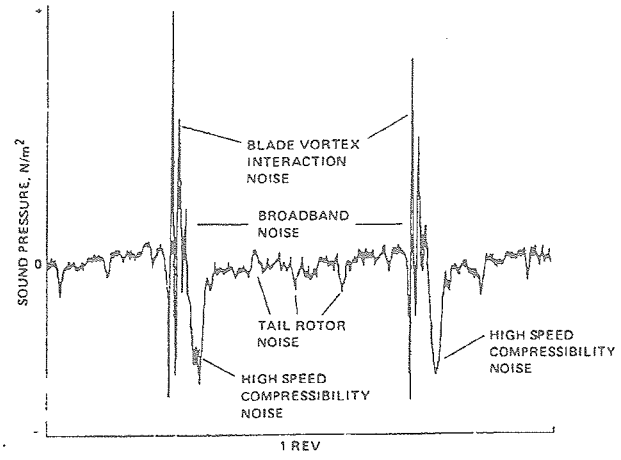

Figure 1.4 Typical BVI noise pattern [5]

of Germany[12], ONERA of France[13], and ATIC of Japan, respectively[14]. Tadghighi et al. [15] developed a procedure for BVI noise prediction, based on a coupling among a lifting-line code (to provide the vortex wake geometry), a three-dimensional unsteady full-potential code (to provide blade surface pressure), and an acoustic code using Farassat's 1A of the Ffowcs Williams and Hawking (FW-H) formulation. Several research groups have been also developing prediction code using various combinations of analytical codes to obtain wake geometry, airload or blade surface pressure, and acoustic signature. Yu et al.[16] summarized the comparisons of the analytical results for Operational Loads Survey (OLS) model rotor. The activity of the BVI working group by Caradonna et al.[17] is also reported, and their work provided a plenty of progress in the helicopter noise research.

BVI is function of many geometrical and aerodynamic parameters, such as hover-tip speed, advance ratio, wake geometry, vortex strength and core size, miss distance, blade deformations, intersection angle and so on. The intensity of the BVI noise is strongly affected by the factors, 1) the local strength of the tip vortex, 2) the core size of the tip vortex, 3) the local interaction angle between the blade and vortex line, and 4) the miss-distance between the vortex and the blade. Each research has approached to one of these parameters to reduce BVI noise.

Passive devices have been considered to suppress high noise levels by rotor tip design and leading edge modification. Many researchers have been trying to

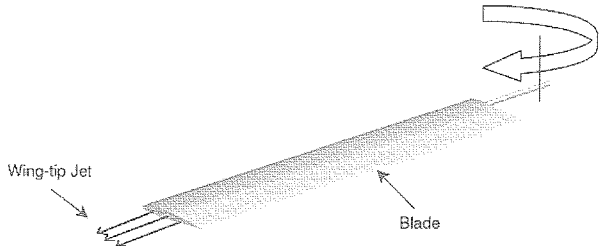

Figure 1.5 Diagram of wing-tip blowing jet of rotor

modify the blade-tip planform to limit shock-wave generation and stall occurrence on the advancing rotor blade.[18, 19] Active devices in BVI noise have been employed such as Individual Blade Control (IBC)[20] method, Higher Harmonic Control (HHC)[21] method and Tailing Edge Flap (TEF)[22] method. These methods are concerned with changing miss distance by disturbing blade or tip vortex. Another way in active control is changing vortex core size or strength using jet-blowing from the tip or attaching Canard wing at the blade tip.[23, 24]

As one of active control methods to reduce the BVI noise, method of jet-blowing from a blade-tip, as shown in Figure 1.5, has been tried by many researchers. The idea of mass injection to control the tip vortex started in the area of fixed wing.

Lee et al.[25–27] have used a wing tip modified with a long single slot to produce a spanwise jet sheet. The effect of this sheet appears to be modification of the lift distribution similar to that produced by an increase in aspect ratio. Unfortunately, the fundamental natures of the tip vortex for the modified wing do not appear to be appreciably altered. Wu and Vakili[28–31] examined the use of discrete wingtip jets for fixed wing to disperse the wake vortex. They have shown that the concept of discrete jets has the potential to effectively disperse the vorticity present in the coherent wing tip vortices. The mechanism for the change appeared to be the formation of multiple auxiliary vortices that decreased the tip vortex strength and introduced increased instability into the flow field. Gowanlock[32] and etc. and other many researchers conducted experimental studies to show jet blowing from a blade-tip can be effective in reducing the strength and velocity gradients of tip vortices. Mineck[33] conducted comprehensive experimental and analytical studies to assess the potential aerodynamic benefits from spanwise blowing at the tip of a moderate-aspect-

swept wing.

For the application to helicopter rotor blade, Tan et al.[34] conducted wind tunnel test to reduce BVI noise by blowing compressed air from blade tip of helicopter rotor. They showed that the vortex intensity is reduced while the vortex location is moved outward which resulted in lower BVI noise level. Yamada[35] conducted parametric study using three-dimensional compressible Euler code to calculate the effect of blowing air from blade tip on the tip vortex of single fixed or rotary blade at the various free stream velocities and blowing conditions, such as injection angle, mass flow rate of jet blowing. Yang et al.[36] conducted comprehensive numerical and experimental investigation of the lateral tip-blowing to reduce BVI noise. The results showed that blowing from the wing-tip can diffuse the tip vortex and displace it outward causing the increased 'wing-span'.

The flow field near the rotor must be quantified to fully develop the understanding of the physics of BVI phenomena. Various studies have been carried out by many researchers in the aerodynamic analysis of the helicopter rotor such as the momentum (energy) method by Rankine and Froude, the vortex lattice method and the lifting surface method based on the potential and vortex theory, the methods using the transonic small disturbance equations[37] and advanced full potential equations[38]. However, unlike the Euler and Navier-Stokes equations, these equations cannot take into account the transport of vorticity, the roll-up of the wake following the blade and contraction of tip vortex past the blade, so they are less perfect model for the prediction of aerodynamic loads on rotor blades.

Since the computing power has been increased progressively over the last two decades, the analysis of helicopter rotor flows in hover and forward flight has progressed from the solution of transonic small perturbation equations and full potential equations to that of Euler equations and more recently to that of Navier-Stokes equations. The recent numerical simulation of the flow in the tip region of a transonic swept wing was performed by Mansour[39], and by Kaynak et al.[40] extended to three-dimensional shock-induced separation using a multiblock Euler/Navier-Stokes zonal method. Later Srinivasan[41] have extended the simulation of the flowfield and the vortex-formation around the wing tip region to the transonic flow.

The three-dimensional flow field round a helicopter rotor blade can be characterized mainly in a tip vortex generated at the tip of a rotor blade and a rotating effect by the rotation of the rotor. The tip vortex generated in the backward vortex of a fixed wing of a helicopter rotor blade has a great importance with an aerodynamical view. Since this tip vortex generally occurs in a complex three-dimensional separating flow which is difficult to analyze, most theoritical or experimental researchers have been trying to understand qualitatively the structure of a vorticity transport from a boundary layer near the wing surface to trailing concentrated vortex. The tip vortex is known to cause not only flow instability such as a sudden decrease of an induced drag or a stall in boundary layer but also acoustic noise. Especially in the rotating blades such as propellers or helicopter rotors, more complex vortical wake is occurred by the interaction of following blade than the fixed wing.

1.3 Motivations and Objectives

In the previous paper, Numerical Study on the Latreal Jet Flow of Helicopter: Part I. Tip Vortex of Fixed Wing, three-dimensional compressible Euler/Navier-Stokes solver are solved to calculate the effect of blowing air from blade tip on the tip vortex of fixed single blade. The numerical results included the position of the vortex center along the vortical flow, the size and strength of the rolled tip vortex, and circulation and maximum tangential velocity of the tip vortex. It showed that the jet blowing from the wing tip can diffuse the tip vortex in the way to make larger core sizes and less velocity gradients, which can be effective way to reduce BVI noise of the rotary wing.

Main objective of this research work is to study on lateral tip-jet blowing as one of method to reduce BVI noise using compressible flow solver with overlapped grid system. For this purpose, first numerical analysis technique will be constructed to solve the BVI phenomena of the helicopter rotor in forward flight. Quantitative calculation will be compared with experimental data. Then using the code developed, BVI analysis will be conducted with various jet blowing conditions to construct database of predicting optimal condition. The numerical results include the position of the vortex center along the vortical flow, the size and strength of the rolled tip vortex, and circulation and

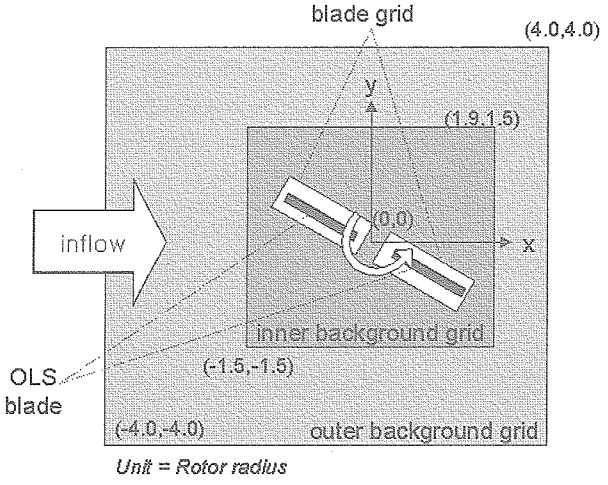

Figure 2.1 Geometric dimensions of computational domain of inner and outer background grid

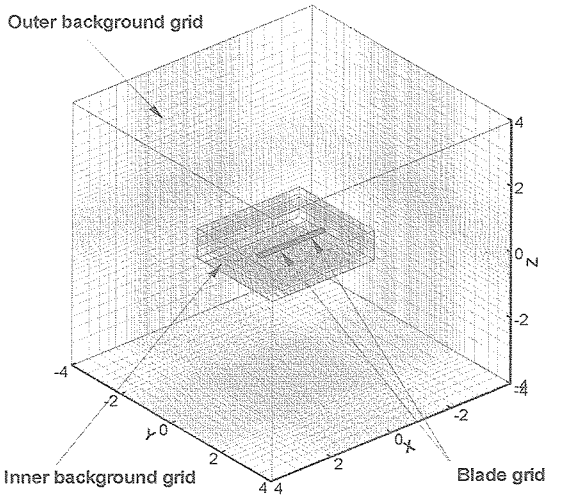

(a) three kinds of grid system

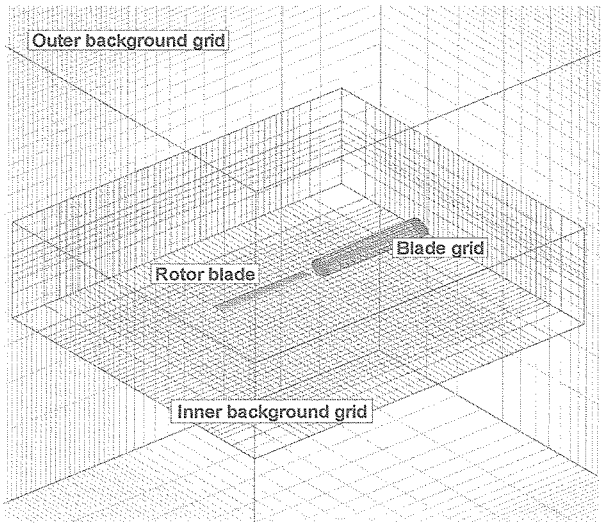

(b) zoomed view of blade grid and inner background grid

Figure 2.2 Whole grid system including blade grids, inner background grid, and outer background grid

maximum tangential velocity of the tip vortex.

This research is conducted as a collaborative research program between National Aerospace Laboratory (NAL) in Japan and Pohang University of Science and Technology (POSTECH) in Korea.

2. NUMERICAL METHODS

2.1 Overlapped grid system of two blades

The predictions of Blade-Vortex Interaction (BVI) noise are performed using a combined method of an unsteady Euler code with an aeroacoustic code based on Ffowcs-Williams and Hawkings formulation. A moving overlapped grid system with three types of grids (blade grid, inner and outer background grid) is used to simulate BVI of helicopter with two OLS-airfoil blades in forward/ descending flight condition. Figure 2.1 shows the computational domain for three types of grid and the geometric dimensions for whole domain. The blade grid rotates in the Cartesian background grid. The Cartesian background grid is divided into the two parts as shown in Figure 2.2. One is the inner background grid and the other is the outer background grid. The inner background grid is placed around the rotor disk, and the outer background grid covers whole computation region with sparse grid density. The calculated flow data are exchanged between inner and outer background grids during calculation steps. Huge numbers of grid points are distributed to the inner background grid to achieve higher resolution, because the density of grid directly affects the strength of numerical viscosity.

The body-fitted blade grid in O-H topology, which is shown in Figure 2.3, moves with the blade motion including rotation, flapping, feathering, and lagging. The inner background grid in Cartesian system is placed around rotor disk to include blade grid. The flow data are exchanged between the blade grids and the inner background grid at the outer boundary of the blade grids. The number of grid points in span-wise direction is considerably increased to match the grid density of the blade grid with that of the inner background grid. The size of the blade grid in normal direction is nearly equal to the chord length as shown in Figure 2.4. Table 2.1 shows the numbers of grid points for each grid system. Two different inner background grids (fine and coarse)

are constructed for testing the grid dependency. The grid spacing of the inner background grid corresponds to 0.11c (fine) and 0.19c (coarse), where c is the chord length. The outer background grid in Cartesian system covers all computational domain, including inner background grid and blade grid.

The dynamic blade motions such as flapping, feathering, and lagging are defined by the input data. These input data can include azimuth-wise data or 1st harmonic function data obtained by measurements or other codes, such as CAMRADII (Comprehensive Analytical Code for Rotorcraft Aerodynamics and Dynamics)[42]. In the present calculation, the collective pitch, cyclic pitch, flapping, and lagging angles measured by the wind tunnel experiment by ATIC are used as the input data. The inertial forces by these dynamic motions have not considered yet in the present calculations.

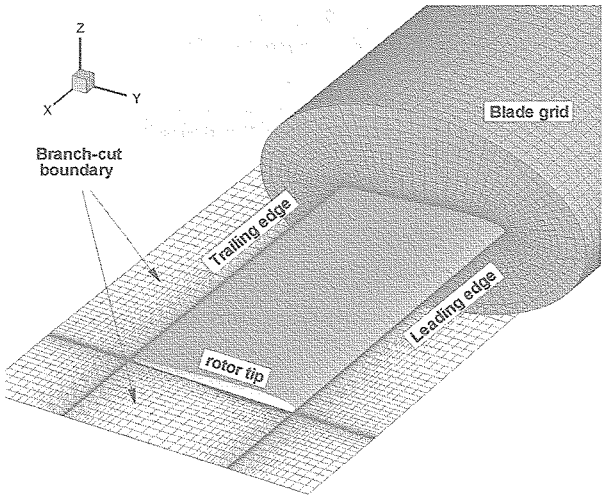

Figure 2.3 Cross section of blade grid and boundary condition

The calculation procedure is shown in the diagram of Figure 2.5. The search and interpolation to exchange flow data, $Q = (r, ru, rv, rw, e)$, between three different grids are executed in each time step because the blade grid rotates with the rotor blade in the background grids. The computation time spent for search and interpolation is one of the disadvantages of the moving overlapped grid approach. In our computation, this problem is severe because a vector and parallel computer is used. Therefore, a new algorithm using tri-liner interpolation is developed and it is vectorized and paralellized[43]. The typical calculation time for the interpolation costs upto about 20% of all calculation time in the parallel computation of 2-bladed rotor case.

The pressure distribution on the blade surface calculated by the CFD code is stored every 0.5 degrees in azimuth-wise direction as the input data in noise calculation. The aeroacoustic code is based on the FW-H formulation without the quadruple terms, which is discussed in the following section.

Only the detailed procedure of the data exchange from the blade grid to background grid is described here. The other procedure of the data exchange from the Cartesian background grid to the blade grid is easier than that from the blade grid to the background grid.

Figure 2.6 shows the procedure of new search and interpolation algorithm. In the first step, the grid indexed (i, j, k) of the background grid point that might be inside of the each blade cell are listed. In the second step, the

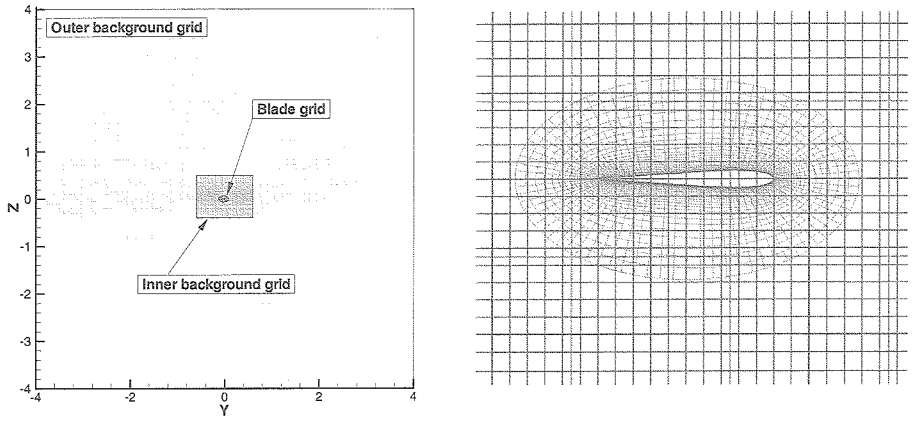

(a) for whole grid system *(b) for blade and inner background grid*

Figure 2.4 Cross section of blade grid and inner background grid

Table 2.1 Specifications of grid systems

Grid	Fine grid	Coarse grid
Inner Background grid	(x × y × z) 450 × 400 × 80 = 14,400,000	(x × y × z) 290 × 230 × 50 = 3,335,000
Outer Background grid	(x × y × z) 83 × 79 × 49 = 321,293	
Blade grid	(chord × normal × span) × blade (81 × 34 × 140) × 2 = 771,120	
Total	15,492,413 points	4,427,413 points
Grid spacing of Inner background Grid in rotor disk	0.11c (=0.006R)	0.19c (=0.0105R)

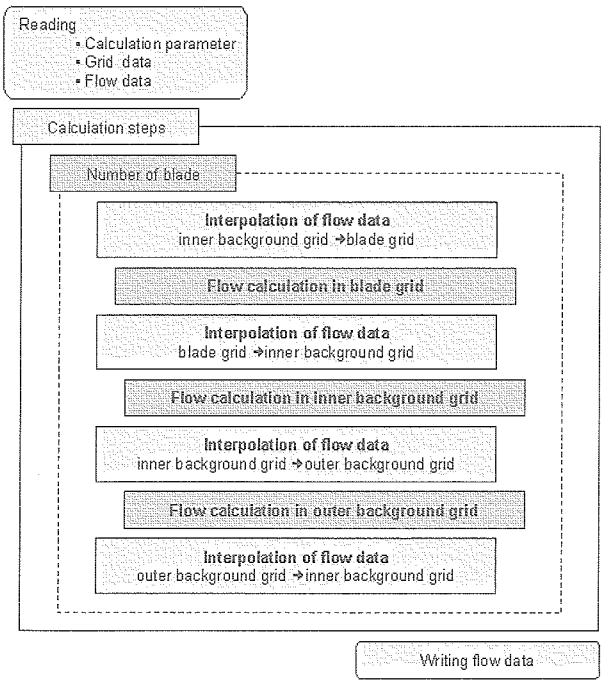

Figure 2.5 Diagram of procedure for flow calculation

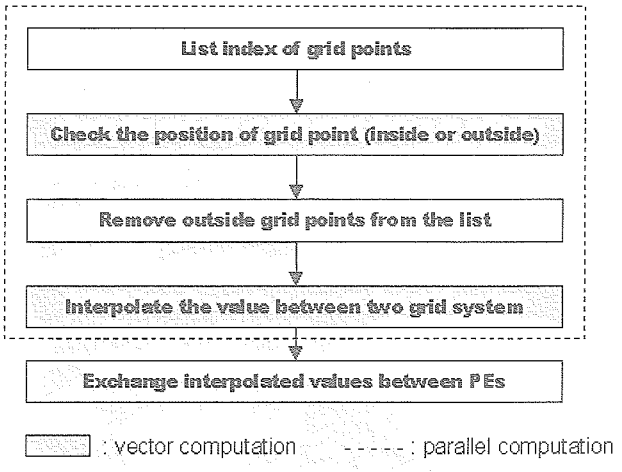

Figure 2.6 Procedure of new search and interpolation algorithm

listed indexes are checked whether they are located inside or outside of the grid cell. The position of the point is expressed by three scalar parameters, s, t, and u for the use of tri-linear interpolation. In this step, values of s, t, and u for each index are calculated. When all s, t, and u are between zero and one, the point is judged to be located inside of the cell.

Figure 2.7 shows bi-linear interpolation for simplicity. Then the grid points outside of the cell are removed from the list and the flow data are interpolated to temporal array. The each processing element (PE) of the supercomputer NWT performs these procedures in parallel. Finally, the interpolated values are exchanged between the processing elements. [44]

2.2 Compressible Euler solver

The general governing forms of three-dimensional compressible Euler equations can be written in generalized coordinate system as the followings.

$$\frac{\partial Q}{\partial t} + \frac{\partial F_i}{\partial \xi_i} H = 0$$

where

$$Q = J^{-1}\begin{Bmatrix} \rho \\ \rho u_1 \\ \rho u_2 \\ \rho u_3 \\ e \end{Bmatrix}, \quad F = J^{-1}\begin{Bmatrix} \rho U_i \\ \rho u_1 U_i + \xi_{i,1} p \\ \rho u_2 U_i + \xi_{i,1} p \\ \rho u_3 U_i + \xi_{i,1} p \\ (e+p)U_i - \xi_{i,t} p \end{Bmatrix}, \quad H = J^{-1}\begin{Bmatrix} 0 \\ -\rho\Omega u_2 \\ \rho\Omega u_1 \\ 0 \\ 0 \end{Bmatrix}$$

In these equations,

$$( )_{,t} = \partial / \partial t, \qquad ( )_{,j} = \partial / \partial x_j,$$
$$(x_1, x_2, x_3) = (x, y, z), \qquad (\xi_1, \xi_2, \xi_3) = (\xi, \eta, \zeta),$$
$$(u_1, u_2, u_3) = (u, v, w), \qquad (U_1, U_2, U_3) = (U, V, W),$$

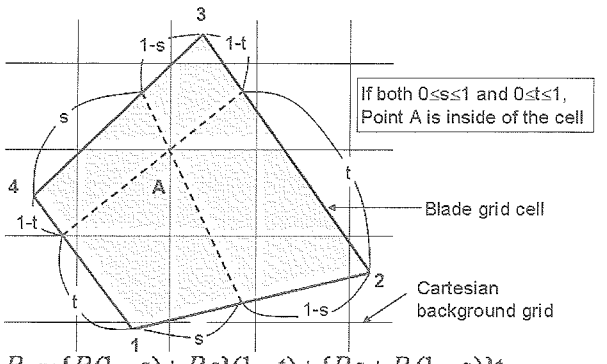

$$P_A = \{P_1(1-s)+P_2 s\}(1-t)+\{P_3 s+P_4(1-s)\}t$$
$$= \{P_1 - P_2 + P_3 - P_4)st + (-P_1 + P_2)s + (-P_1 + P_4)t + P_1$$

Figure 2.7 Diagram of bi-linear interpolation for overlapped grid system

And the Jacobian of the transformation is

$$J = \frac{\partial(\xi,\eta,\zeta)}{\partial(x,y,z)} = \left[x_\xi\left(y_\eta z_\zeta - y_\zeta z_\eta\right) - x_\eta\left(y_\xi z_\zeta - y_\zeta z_\xi\right) + x_\zeta\left(y_\xi z_\eta - y_\eta z_\xi\right)\right]^{-1}$$

In the above equations, p is the gas density, u, v, w, the Cartesian velocity components in x, y, z directions, and U, V, W are components of contravariant velocity. The quantity Ω is the angular velocity of the blade rotation, and e is the total energy per unit volume. The pressure p is obtained by the perfect gas equation by

$$p = (\gamma - 1)\left[e - \frac{1}{2}\rho\left(u^2 + v^2 + w^2\right)\right]$$

where γ is the ratio of specific heats, usually as $\gamma = 1.4$ for air.

The inviscid flux vectors are discretized using Roe's flux difference splitting (FDS) method[45]. The flux difference across a cell interface is divided into components associated with each characteristic wave with third order accuracy using TVD scheme.[46] TVD scheme has a good capability of capturing the shock wave without adding artificial dissipation. Roe's approximate Riemann solver does not satisfy the entropy condition and thus permits physically inadmissible expansion shock. To remedy this problem, entropy correction is applied [47]. In addition, an upwind scheme based on TVD by Chakravarthy and Osher[48] is applied for the inviscid terms of the explicit right-hand-side. Each operator is decomposed into the product of lower and upper bi-diagonal matrices by using diagonally dominant factorization. The accuracy of this solver in space and in time is 2nd-order and 1st-order, respectively.

For time integration, Euler Backward Implicit Time Integration is used in the conventional delta form. In order to obtain the unsteady solution in the forward flight condition of helicopter rotor, the Newton iterative method is applied. In this method, the above-mentioned scheme

$$LHS\left(Q^{n+1} - Q^n\right) = -\Delta t RHS$$

is modified as

$$LHS^m\left(Q^{m+1} - Q^m\right) = -\Delta t\left(\frac{Q^m - Q^n}{\Delta t} + RHS^m\right)$$

where m means the number of the Newton iteration.

In order to reduce the residual, six times sub-iterations are used at each time-step. The typical dividing number along the azimuthal direction is about 9000 per revolution for the fine grid and 4500 for the coarse grid. It corresponds to azimuth angles about 0.04° and 0.08° per step, respectively. The unsteady calculation is impulsively started from the azimuth angle of 0°. From the previous research, the starting vortex can be negligible in forward flight calculation. For the fixed wing calculation, the same numerical scheme is used for a single blade.

Background Cartesian grid, which has relatively coarse grid spacing compared to the blade grid, uses a high accuracy explicit scheme to maintain the strength of tip vortex from blade grid. To contain the movement of tip vortex in wide range, it needs a large computational space, i.e. a high computing cost. By using high accuracy scheme for Cartesian grid in the background grid, we can save computing cost. The compact TVD scheme is employed for spatial discretization[49], and MUSCL cell interface value is modified to achieve 4th-order accuracy. Simple High-resolution Upwind Scheme (SHUS)[50] is employed to obtain numerical flux. SHUS is one of the Advection Upstream Splitting Method (AUSM) type approximate Riemann solvers, which is known to have less numerical diffusion. Among the explicit time integration methods, the four-stage Runge-Kutta method is used for the present calculation. The free stream condition is applied for the outer boundary of the outer background grid.

Numerical Wind tunnel (NWT) of NAL in Japan is used to get an accurate aerodynamic flow solution near the

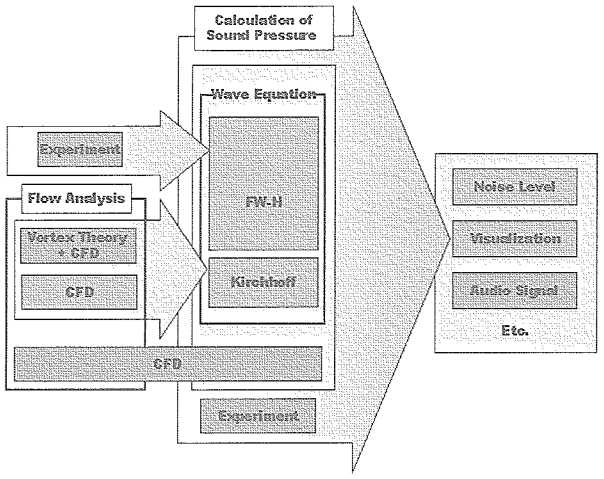

Figure 2.8 Noise Analysis Methods and Procedure [55]

rotor blade. The NWT is a parallel super computer which consists of 166 processing elements (PEs). The performance of an individual PE is 1.7 GFLOPS, and each PE has a main memory of 256MB. High-speed cross-bar network connects 166 PEs to make the total peak performance to be about 280 GFLOPS and the total capacity of main memory as much as 45GB. For the calculation of this paper, the typical dividing number along the azimuthal direction is about 2000/rev. The NWT makes it possible to conduct parametric study of the effect of the lateral jet blowing on the intensity of the BVI noise. It takes about one week to obtain a fully converged solution of a rotor Euler calculation with about 15 million grid points using 36CPUs.

2.3 Far-field acoustic prediction method

The prediction method of the far field acoustic pressure is based on the combined method of CFD technique with acoustic equation solver. The prediction method of rotor noise is composed of three steps: calculation of sound pressure of the noise source, acoustic prediction computation at the observer position, and post-processing of the noise data in the way of sound level, visualization or audible converting. Figure 2.8[51] shows the diagram of noise analysis procedure and acoustic prediction methods.

Several prediction methods are available. Direct computation can be used to get the noise solution directly from the flow calculation with CFD based methods, but this is available only near field, and best way is the coupled with integral method for far-field prediction. Acoustic Analogy, which is re-arranged in to Ffowcs Williams?Hawkings Equation and Kirchhoff formula are widely used and still under construction for better applications.

The idea of Lighthill's acoustic analogy[52] starts from the rearrange governing equation into a wave equation as following.[53–55]

$$\frac{\partial}{\partial t}\left\{\frac{\partial \rho}{\partial t}+\frac{\partial \rho u_i}{\partial x_i}\right\}=0 \quad \text{cintinuily}$$

$$-\frac{\partial}{\partial x_i}\left\{\frac{\partial \rho u_i}{\partial t}+\frac{\partial}{\partial x_i}\left(\rho u_i u_j+P_{ij}\right)\right\}=0 \quad \text{momentum (N-S)} \blacktriangleright\blacktriangleright\blacktriangleright$$

$$\frac{\partial^2 \rho}{\partial t^2}=\frac{\partial^2}{\partial x_i \partial x_j}\left(\rho u_i u_j+P_{ij}\right)$$

$$\frac{\partial^2 \rho}{\partial t^2}-c_0\frac{\partial^2 \rho}{\partial x_i \partial x_j}=\frac{\partial^2 T_{ij}}{\partial x_i \partial x_j}$$

where

$$T_{ij}=\rho u_i u_j+P_{ij}-c_0\rho\delta_{ij}$$

Ffowcs-Williams and Hawkings source contributions linearly superimpose as

$$p'(\vec{x},t)=p_t'(\vec{x},t)+p_l'(\vec{x},t)+p_q'(\vec{x},t)$$

to develop quadrupole source prediction independently, and can identify contributions from each source. Ffowcs-Williams and Hawkings formulation without quadruple term can be expressed in integral form.

$$p(x,t)=\frac{1}{4\pi}\left(\frac{\partial}{\partial t}\int\frac{\rho_0 v_n}{r\Lambda}d\Sigma+\frac{1}{c_0}\frac{\partial}{\partial t}\int\frac{p_b\cos\theta}{r\Lambda}d\Sigma+\int\frac{p_b\cos\theta}{r^2\Lambda}d\Sigma+\frac{\partial^2}{\partial x_i\partial x_j}\int\frac{T_{ij}}{r\Lambda}dV\right)$$

$$\Lambda=\sqrt{1+M_n^2-2M_n\cos\theta}$$

$T_{ij}=\rho v_i v_j+p_{ij}-c_0^2(\rho-\rho_0)\delta_{ij}$; Lighthill's stress tensor

Retarded time solution to Ffowcs-Williams and Hawkings equation, neglecting quadruple noise, can be written in the following equations,

$$4\pi p'(\vec{x},t)=\frac{\partial}{\partial t}\int_{f=0}\left[\frac{Q}{r(1-M_r)}\right]_{ret}ds+\frac{\partial}{\partial x_j}\int_{f=0}\left[\frac{L_i}{r(1-M_r)}\right]_{ret}ds$$

as the form of [56]

$$4\pi p'(\vec{x},t)=\int_{f=0}\left[\frac{\dot{Q}+\dot{L}_r/c}{r(1-M_r)^2}\right]_{ret}ds+\int_{f=0}\left[\frac{L_r-L_M}{r^2(1-M_r)^2}\right]_{ret}ds$$

$$+\int_{f=0}\left[\frac{(Q+\dot{L}_r/c)(r\dot{M}_r+c(M_r-M^2))}{r^2(1-M_r)^3}\right]_{ret}ds$$

or

$$4\pi p'(\vec{x},t)=\int_{f=0}\left[\frac{\rho_0(\dot{v}_n+\dot{v}_h)+\dot{L}_r/c}{r(1-M_r)^2}\right]_{ret}ds+\int_{f=0}\left[\frac{L_r-L_M}{r^2(1-M_r)^2}\right]_{ret}ds$$

$$+\int_{f=0}\left[\frac{(\rho_0 v_n+\dot{L}_r/c)(r\dot{M}_r+c(M_r-M^2))}{r^2(1-M_r)^3}\right]_{ret}ds$$

where

$p'(\vec{x},t)$: acoustic pressure at position $\vec{x}$ and at time t

L_i : components of the local force intensity acting on the fluid

M : Mach number according to freestream sound speed, c

r : distance from the observer $\vec{x}$ to the source position $\vec{y}$

$$L_r = L_i r_i,\ \dot{L}_r = \dot{L}_i r_i,\ L_i = P_{ij} n_j,\ L_M = L_i v_i / c,$$
$$c,\ \dot{M}_r = v_i r_i / c,\ Q = \rho_0 v_n = \rho_0 v_n = \rho_0 v_i n_i$$

where

(1) subscript r and n indicate a dot product of the main quantity with unit vectors in the radiation and surface normal directions, respectively

(2) dot over variables indicates source-time differentiation

(3) $[\ ]_{\text{ret}}$ indicates the integrands are evaluated at the retarded (emission) time

in 4 different noises:

$$\left[\frac{\dot{L}_r / c}{r(1-M_r)^2} + \frac{L_r / c \cdot \dot{M}_r}{r(1-M_r)^3}\right] ds \quad : \text{loading noise (far field)}$$

$$\left[\frac{L_r - L_M}{r^2(1-M_r)^2} + \frac{L_r(M_r - M^2)}{r^2(1-M_r)^3}\right] ds : \text{loading noise (near field)}$$

$$\left[\frac{\rho_0(\dot{v}_n + v_{\dot{n}})}{r(1-M_r)^2} + \frac{\rho_0 v_n \cdot r\dot{M}_r}{r^2(1-M_r)^3}\right] ds : \text{thickness noise (far field)}$$

$$\left[\frac{\rho_0 v_n c(M_r - M^2)}{r^2(1-M_r)^3}\right] ds : \text{thickness noise (near field)}$$

Hypothesis of Ffowcs-Williams and Hawkings equation[57] to be satisfied are known that the noise source must lay in low speed flow, and viscous and turbulent stress contribution should be negligible with respect to pressure on the body surface. Also observer should be located outside source region (i.e. outside boundary layer, separation flow or wake) in order to avoid the nonlinear effect. In most cases, observer is assumed to move in the same direction and at the same speed of the moving body to keep the constant distance between the observer and the moving body.

3. RESULTS: Jet Blowing with Two Blades

3.1 Comparisons with experimental data

Numerical computations are performed by the present method for the realistic rotor system, which was tested in the anechoic Neutsch-Niederlaendischer Windkanal (DNW). Acoustic data have documented the blade vortex interaction (BVI) impulsive noise radiated from a 1/7-scale model main rotor of AH-1 series helicopter. The model rotor of two blades with high aspect ratio is designed to duplicate the AH1-OLS full-scale, pressure-instrumented blades, which also have been used for full-scale aerodynamics and noise testing by NASA.[58] The thickness and chord of the full-scale 540 rotor blade are increased slightly (4% and 5%, respectively) to accommodate surface-pressure transducers, thus defining OLS airfoil shape. The characteristics of the model rotor OLS blade of 1.916m diameter (6.6ft) are shown in Fig. 3.1. The whole rotor test system mounted in the DNW open test section is schematically shown in Appendix.

The dimension of the calculated rotor and the operating conditions are summarized in Tables 3.1. Three cases of shaft tilt angle are selected to evaluate the capability of our code to predict BVI noise. The shaft tilt angles are corrected by the Heyson's method [59]. Table 3.2 shows many operating conditions for experiments and three test cases which are selected as numerical calculation. Even the most critical BVI phenomena, which are marked in black-filled circle, cannot be calculated because of numerical instability, the three test cases (**case 1, 2, 3**) are known to show the physics of BVI phenomena and noise peak successfully. In the following calculation of jet blowing with two blades in forward flight, the **case 1** will be used on account of its

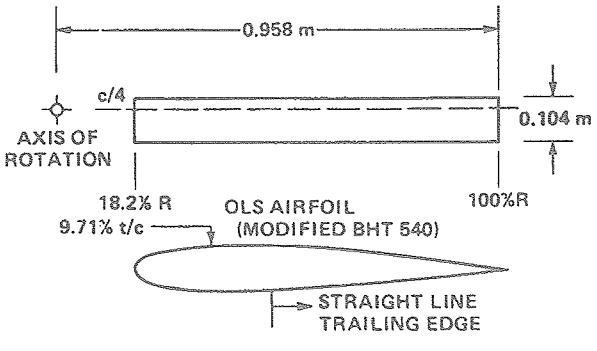

Figure 3.1 Geometric dimensions of OLS model rotor

Table 3.1 Operating conditions

Tip Mach Number, M_H	0.664
Advance ratio, μ	0.164
Tip path plane angle	3.0
Collective pitch angle, θ_{m0}	5.20
Cyclic pitch angle, θ_{mc}	2.72

Table 3.2 Operating conditions for experiment and calculation

tip path plan angle	μ=0.164 M_H=0.664 C_T=0.0054 M_{AT}=0.773	μ=0.194 M_H=0.664 C_T=0.0054 M_{AT}=0.793	μ=0.224 M_H=0.664 C_T=0.0054 M_{AT}=0.813	μ=0.270 M_H=0.664 C_T=0.0054 M_{AT}=0.843
−5	○	○	○	○
−4			○	○
−3		○	○	○
−2	○	○	●	○
−1	○	●	○	○
0	●	○	○	●
1	○	○	○	○
2		○	○	○
3	Case 1	Case 2	Case 3	
4	○	○	○	
5	○			
6				
7	○			
● : largest BVI noise in each condition				

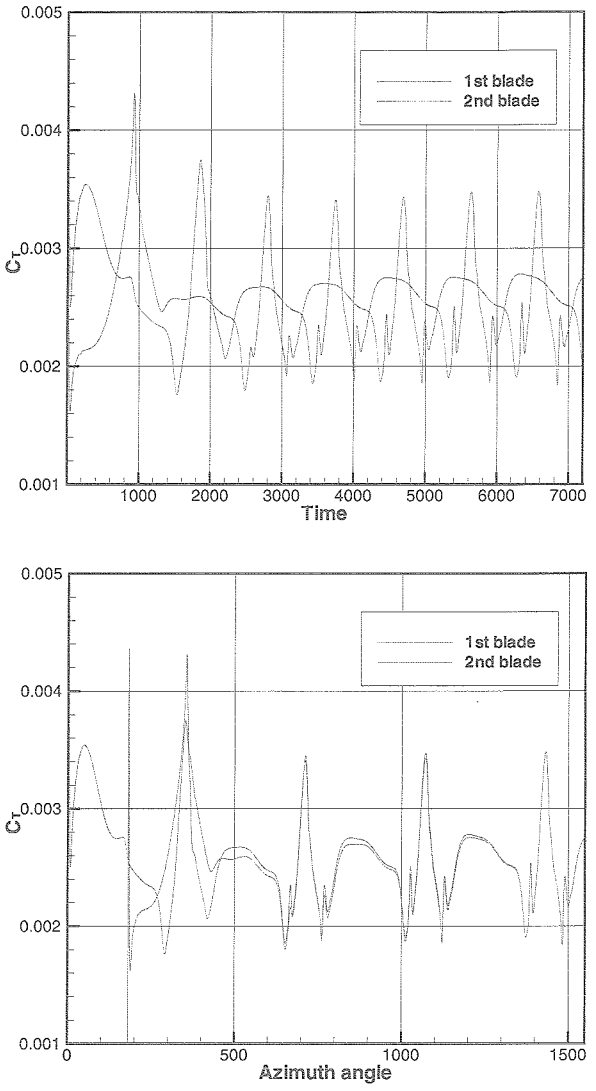

Figure 3.2 Time history of lift coefficients according to rotating time and azimuth angle

high peak value in BVI noise.

These calculations are impulsively started from a free stream condition. The computation is carried out on Numerical Wind Tunnel (NWT) in NAL to perform large scale and accurate computations. NWT is a vector parallel super computer consists of 166 processing elements (PE). Each processing element has a vector processor with 1.7 Gflops peak performance. The CPU time is about 20 hours per revolution using 12 PEs for coarse grid calculation and 30 PEs for fine grid calculation. The periodic solution is obtained after 4 revolutions. The required memory sizes are 3GB and 8GB for the coarse and the fine grid calculations, respectively.

Figure 3.2 shows the time history of lift coefficient at one point on blade surface according to the rotating time and azimuth angle during about 4 revolutions of rotor blade. These calculations are impulsively started from a steady solution using a free stream condition. The history profile of two blade shows phase difference for half revolution, which can be easily predicted from the blade geometry. When the profile get shifted in phase according to the azimuth angle, the peak values of two blades grow to be consistent at the 4th revolution, which indicates that the flow calculation is converged.

Figure 3.3 shows the microphone positions in the experiment. One of thirteen traverse microphones of experiment on the horizontal plane of 2.43m (1.15R) below the center of the rotor are used. The sound pressure level (SPL) is calculated from blade surface pressure using the aeroacoustic code based on the FW-H formulation. The calculated SPL waveform of BVI noise

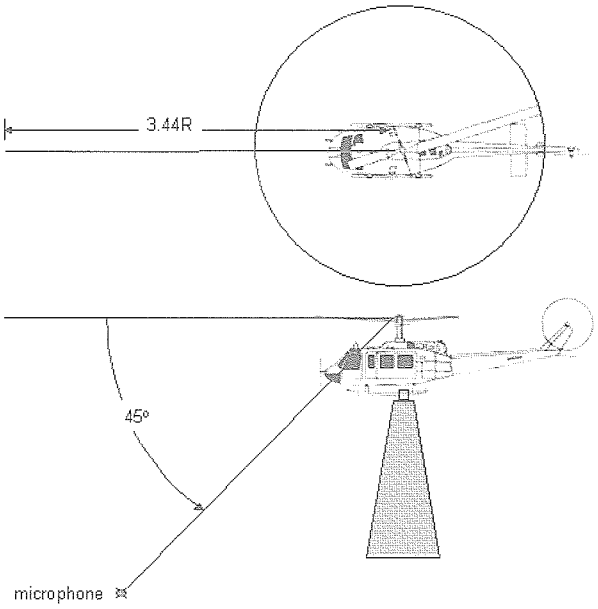

Figure 3.3 Microphone position for noise analysis

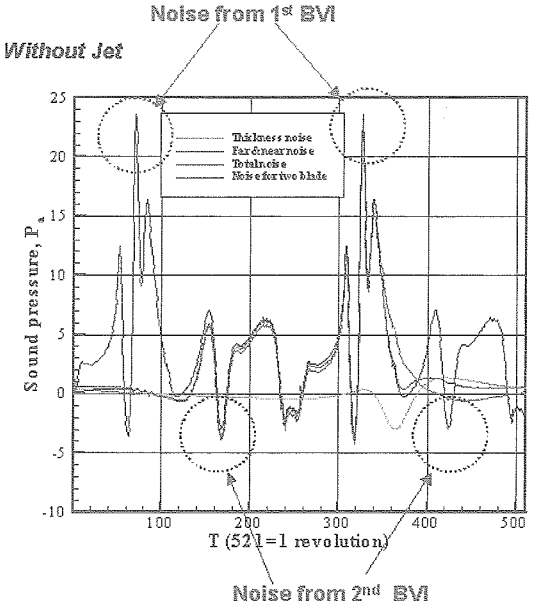

Figure 3.4 Diagram of several noise sources for one revolution

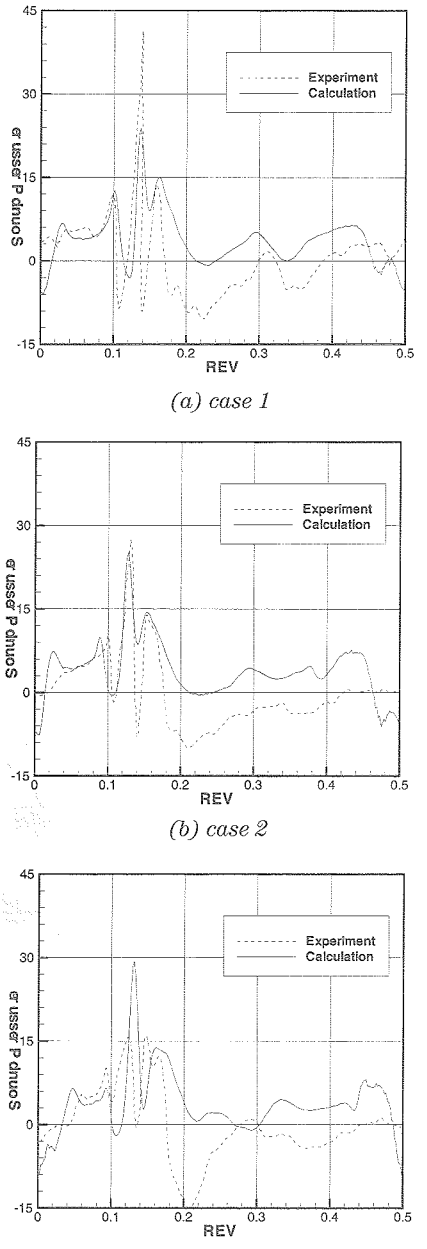

(a) case 1

(b) case 2

(c) case 3

Figure 3.5 Comparison of sound pressure level (SPL) histories between calculation and measurement for case 1,2,3

clearly shows distinct spikes caused by the interaction between blade and vortex. The higher accuracy numerical schemes in background grids and very large-scale computation lead us to these satisfying results. The difference between calculated and measured waveforms is due to the disagreement of intensity and location of BVI. In addition, the azimuthal width of the spike seems to be stretched in the calculated SPL waveform. The reason of the stretch might be the expansion of the core radius of tip vortices. Concerning a core radius of tip vortices, further study will be needed.

Figure 3.4 shows the several kinds of noise sources including thickness noise, far- and near-field noise, and total noise for both single blade and two blades. The magnitude of thickness noise is relatively small when compared to that of far-/near-field noises, and the main noise comes from far field noises which are dominated from blade vortex interaction. Total noise for two blades shows the typical BVI noise pattern for one revolution.

Figure 3.5 shows the comparison of sound pressure

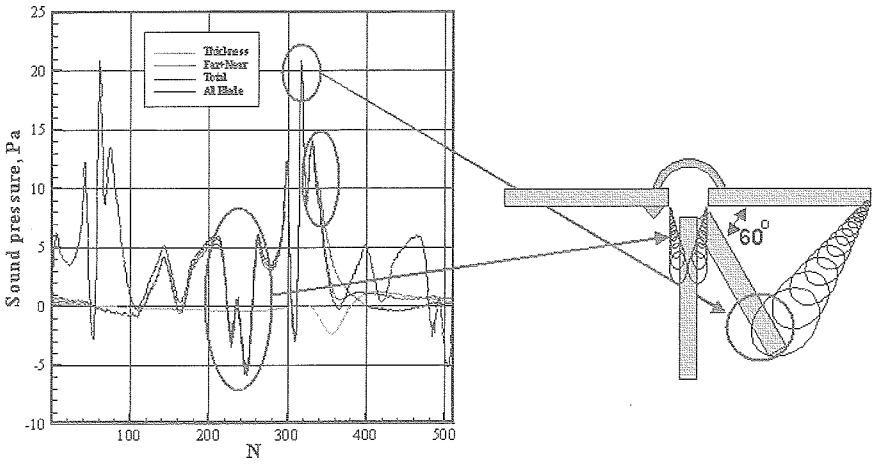

Figure 3.6 Diagram of noise sources for OLS rotor cases

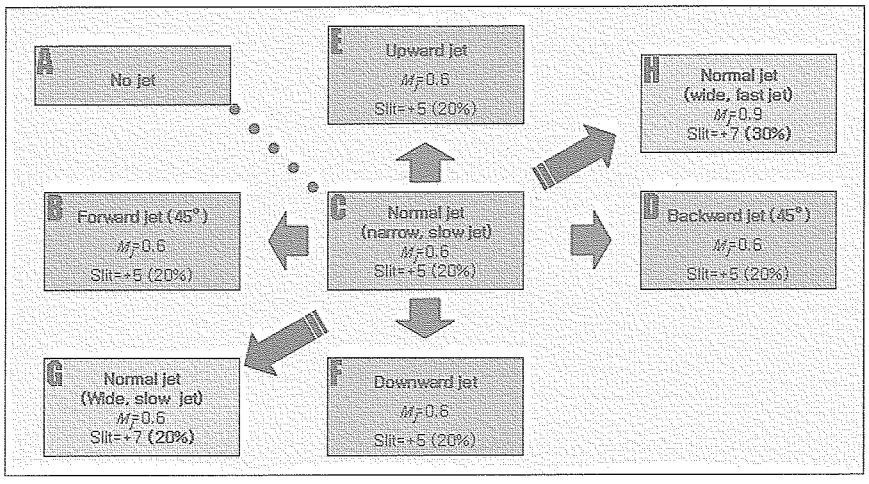

Figure 3.7 Case diagram for various jet conditions in overlapped grid system

level (SPL) histories between measurement and calculation for **case 1, 2, 3** during one revolution of rotor blade respectively. Even the peak values are not exactly correct in magnitude, the calculation show good agreements in the peak position, which implies that the calculation can predict the BVI phenomena for forward flight.

Some explanations of difference of minor peak values in sound pressure level are shown in Fig. 3.6. The highest peak in positive values comes from the main blade vortex interaction, but the lowest peak in negative values is supposed to originate from the interaction between vortex and root tip of the rotor blade. In real or model helicopter, the flow characteristic near root tip region is controlled by the hub system, which is not considered in the calculation.

3.2 Calculation of jet blowing

The predictions of Blade-Vortex Interaction (BVI) noise with various jet conditions are performed using a combined method of an unsteady Euler code with an aeroacoustic code based on Ffowcs-Williams and Hawkings formulation. A moving overlapped grid system with three types of grids (blade grid, inner and outer background grid) is used to simulate BVI of helicopter with two OLS-airfoil blades in forward/ descending flight condition [59]. The model rotor blades are set to be AH1-OLS blades, which also have been used for full-scale aerodynamics and noise testing by NASA. The rotor motion is also set to be one of the test cases of NASA experiment.

Figure 3.7 shows the diagram of cases with various directions of tip jet blowing. Case A is the rotor without

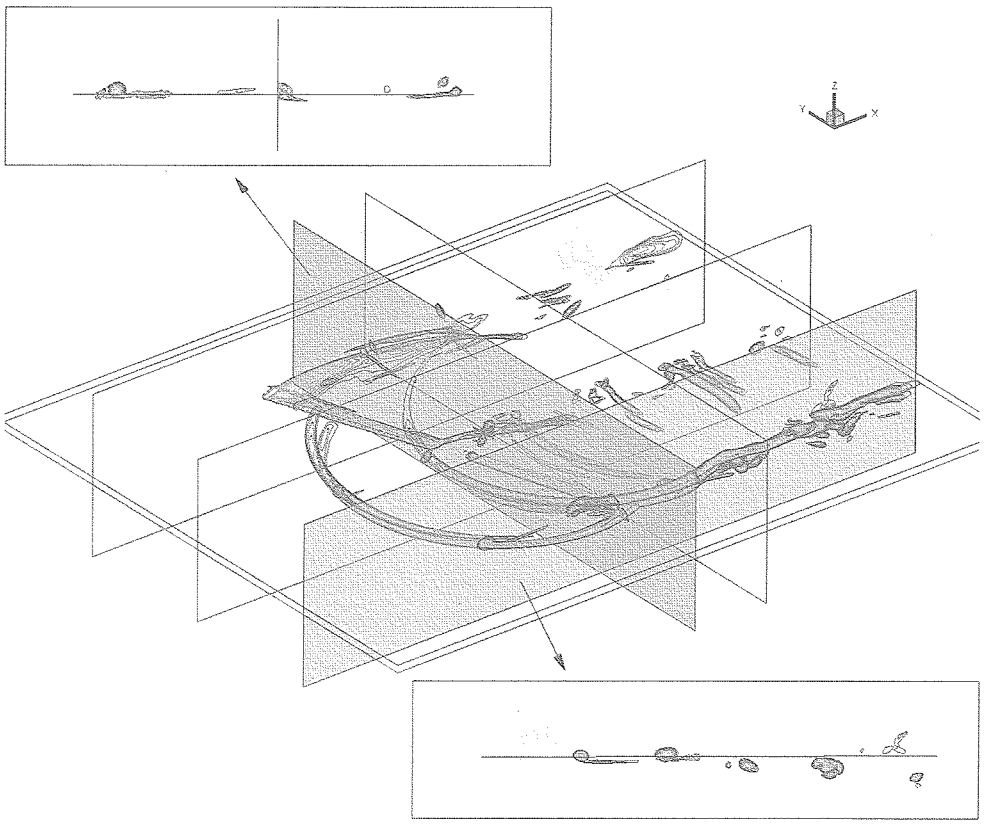

Figure 3.8 Visualized tip vortices of vorticity contours ($M = 0.8$, $M_j = 0.6$, case 1 using coarse grid without jet)

jet blowing, and the various jet blowing condition are applied to from case B to case F. Case B is 45 degrees forward blowing and case D is 45 degrees backward blowing. Case E is 45 degrees upward blowing and case F is 45 degrees downward blowing. To see the effect of blowing volume flow, case G has 2 times larger area of jet slit than that of case C, and case H has both wide jet slit area and higher jet Mach number of 0.9.

Figure 3.8 shows vorticity contour at several sections together to visualize the trace of tip vortex in forward and descend flight condition using coarse grid system at the azimuth angle of near 100 degree. It clearly shows the trace of tip vortex which are generated by two rotor blades, and also shows the interaction of blade and tip vortex. The tip vortex are shown to lasts up to nearly 3~4 revolution causing several interactions with following blades. Near blade root there are another significant tip vortex, which are not supposed to happen in real helicopter system. This extra vortex structure is considered originated from the absence of rotor hub system in computation, which is already mentioned in the previous section.

To see the detail of vortex movement, the contours of vorticity on the plane of several intersectional planes in z-axis are shown in Figure 3.9. Tip vortex generated from two blades in forward and descending flight moves slightly upward, but still remains near the rotation plane (or rotor disk), which makes blade vortex interaction. As mentioned above, from this contour, we can see that the vortex generated from the preceding blade pass through the following blade. Although the critical blade vortex interaction is supposed to occur during direct interaction between vortex and blade at the most front part of the leading edge, it may cause the numerical instability during calculations.

The computed pressure coefficient (C_p) histories on blade surface are plotted in Figure 3.10 for various jet conditions. The fluctuations caused by BVI are successfully captured in the way of sudden changes of pressure coefficient, which are observed in the advancing side (from 0° to 90°) and the retreating side (from 270° to 360°). The reason of the disagreement is the difference of the miss-distance between vortex core and rotor blade in BVI region. In the tip region ($r/R = 97\%$

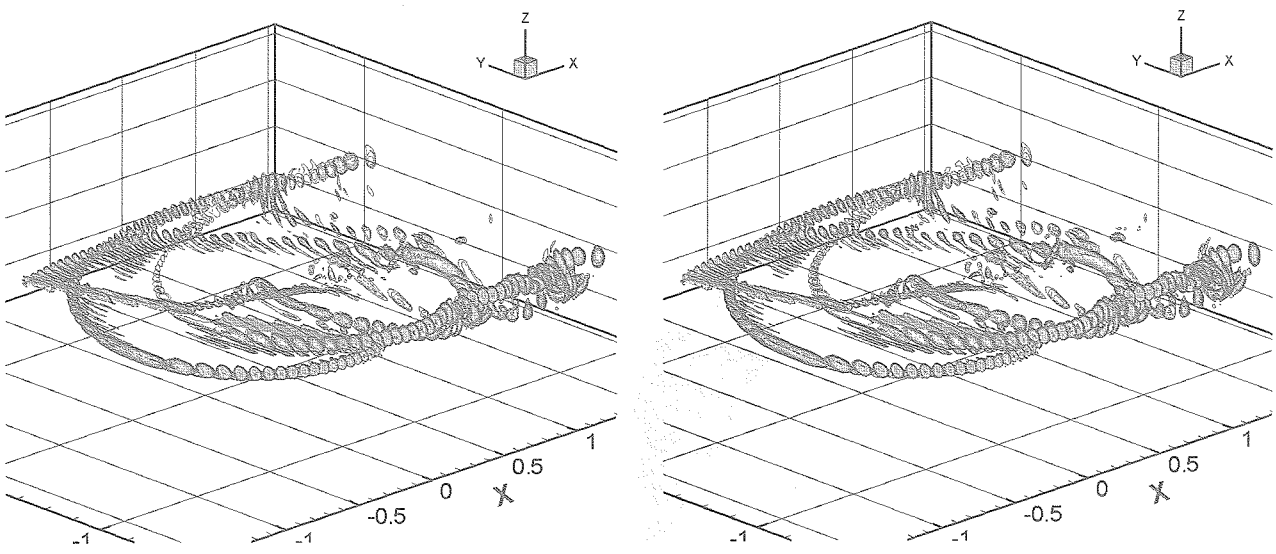

(a) no jet *(b) normal jet*

Figure 3.9 Contours of vorticity on the plane of several sections

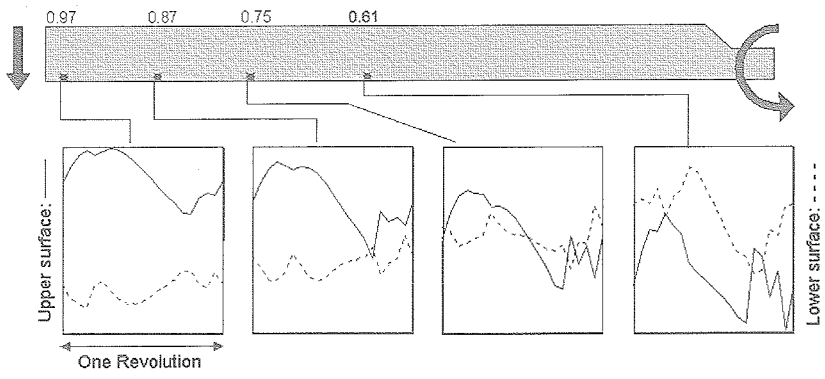

Figure 3.10 Computed pressure coefficient (C_p) histories on blade surface

and 87%), the number of BVI events in the calculation is less than that in the experiment in advancing side. In the middle span station ($r/R = 61\%$), on the other hand, the number of BVI events in the calculation is more than that in the experiment. In addition, the azimuth position of BVI is shifted forward compared with that in the experiment. It can be supposed from these results that the position of calculated tip vortices in the BVI region is lower than that of measured ones. Thus the calculated location where tip vortices intersect the rotor disk might be moved inside and forward compared with the measured one. Consequently, the locations of BVI are not in good agreement. This feature is observed for all three cases. The quantitative discrepancy between calculation and measurement mentioned above is caused by the difference of angle of attack because blade elasticity is not considered in the present code. The discrepancy of miss-distance, which causes quantitative disagreement of the pressure coefficient, is caused by the strong downwash induced by the over-estimation of thrust.

To see the detail of vortex movement at the several sections along tip vortex, the contours of vorticity on the sectional planes are selected in Figure 3.11. Figure 3.11(a) shows the diagram of sectional contours in the perspective view of vorticity contour. Section (a) shows the tip vortex just behind advancing rotor blade, and section (b) shows its development and the other tip vortex at the same time. Section (c) shows the intersection with retreating rotor blade and section (d)

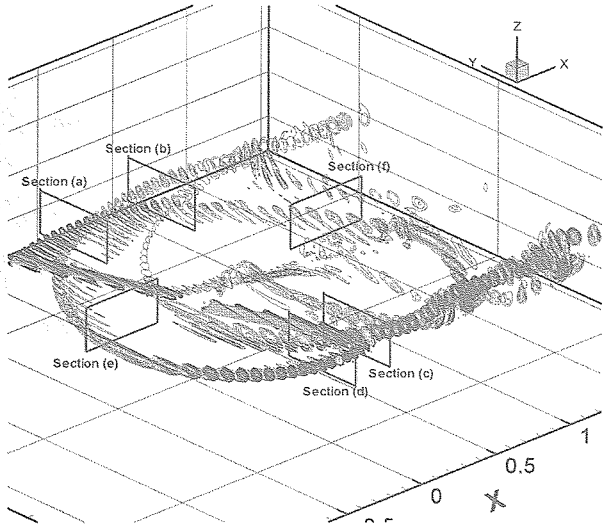

(a) perspective view of vorticity contours

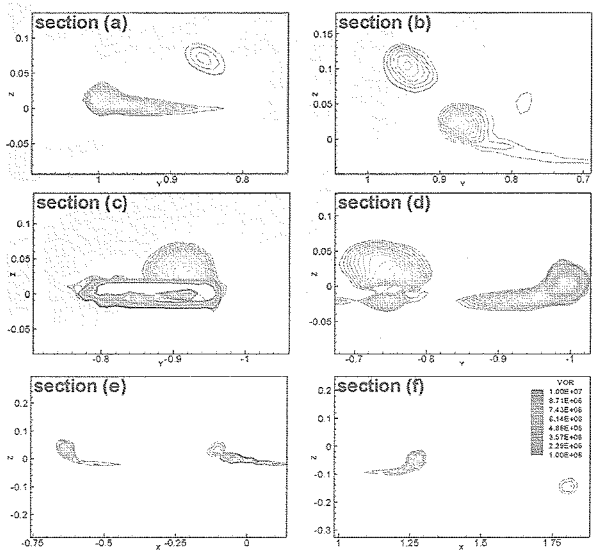

(b) vorticity contours without jet

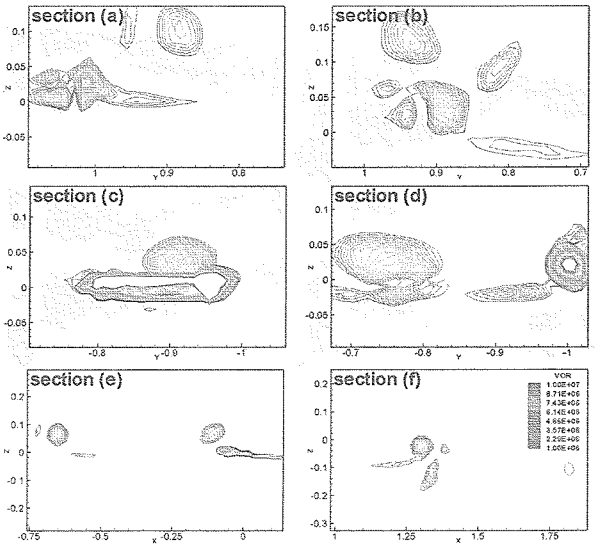

(c) vorticity contours with jet

Figure 3.11 Contours of vorticity on the plane of several sections along tip vortex

shows both the formation of new tip vortex and the break down of old tip vortex. Section (e) and (f) show the sections of middle passage of tip vortex. Figure 3.11(b) shows the vorticity contours at six sections without jet and figure 3.11(c) shows the vorticity contours at six sections with normal, fast, and wide jet.

As shown in figures above, the tip vortices with jet blowing seem more disturbed by jet to produce bigger core size, as illustrated at section(a) and section(d) in figure 3.11(a) and (b). Also the center of tip vortex in the middle of passage, as shown at section (e) and (f) is moves upward, which is especially important in the miss-distance of BVI in section (e). This effect is also seen in section (a), which shows the tip vortex from the previous advancing blade remains upward owing to the jet blowing.

Figure 3.12 shows the diagram and zoomed view near BVI using iso-contour of vorticity of tip vortex. Perspective view of iso-contour of vorticity of tip vortex shows the significant traces of tip vortex in figure 3.12(a). To see the effects of jet blowing at the BVI of advancing blade, zoomed view of vorticity iso-contour near BVI is illustrated in figure 3.12(b).

The iso-contours of vorticity of tip vortex near BVI interaction are illustrated for the case without jet blowing in figure 3.13(a) and for the case with fast, wide

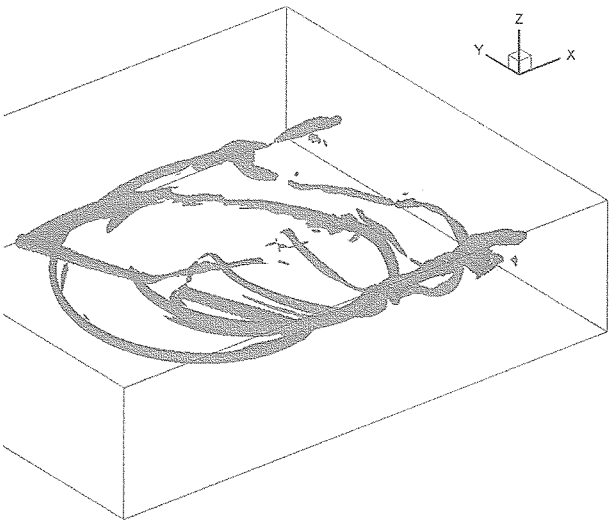

(a) perspective view of iso-contour of vorticity of tip vortex

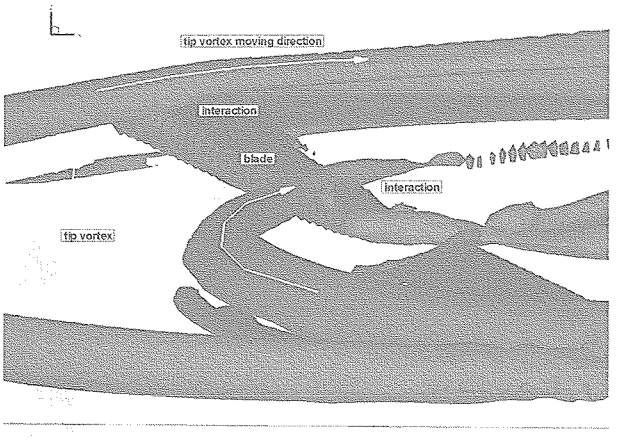

(b) zoomed view near BVI

Figure 3.12 Diagram of zoomed view near BVI using iso-contour of vorticity of tip vortex

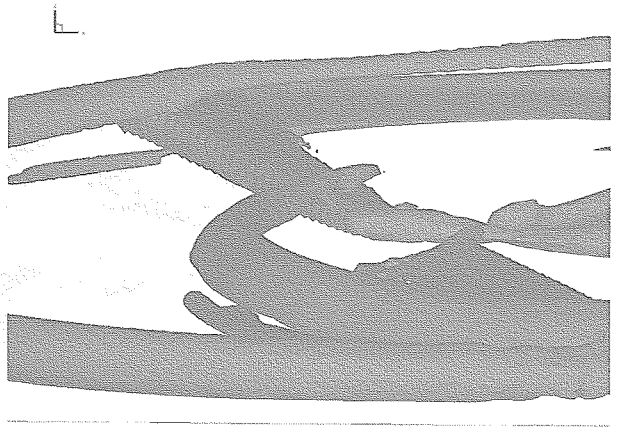

(a) no jet

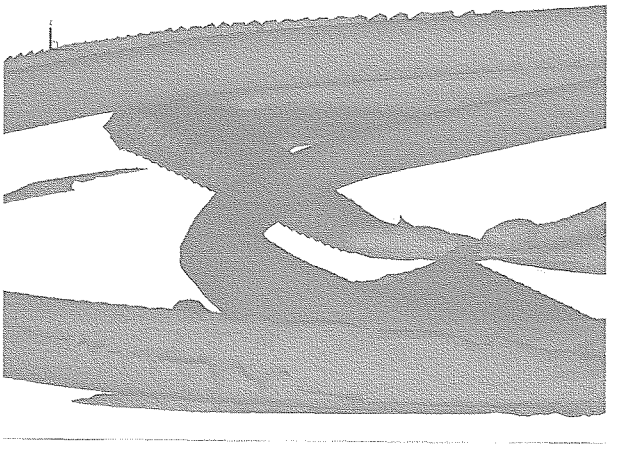

(b) wide fast jet ($M = 0.9$)

Figure 3.13 Iso-contour of vorticity of tip vortex near BVI

jet in figure 3.13(b). The tip vortex with jet shows larger core size, but it seems less disturbed by the interacting blade by keeping its original shape of tip vortex. It means that jet blowing moves the tip vortex upward during interaction to make the tip vortex less disturbed. So jet blowing plays a positive role to reduce BVI noise in both ways: at first, by increasing the core size to produce less pressure gradient during BVI, and at second, by pushing the vortex center upward to increase miss-distance during BVI.

Figure 3.14 shows the pressure coefficient distribution according to azimuth angles for upper and lower blade surface according to the jet conditions. The pressure coefficients show the similar patterns globally in spite of different jet conditions, but small differences near the tip region at both advancing and retreating sides can be detected.

The computed pressure coefficient (C_p) histories on blade surface are plotted in Figure 3.15 with/without jet conditions. To see the global differences of jet effects, the comparison of pressure coefficient (C_p) histories are drawn in Figure 3.16 according to various jet conditions for one revolution at one position near leading edge on upper and lower blade surface. For most jet conditions, the difference occurs at the retreating side (azimuth angles from 270° to 360°) in the tip region ($r/R = 97\%$ and 87%).

Figure 3.17 shows the sectional lift coefficient (C_l) distributions and lift forces along the spanwise direction for azimuth angle, and Figure 3.18 shows the comparison of sectional lift coefficient (C_l) distributions and lift

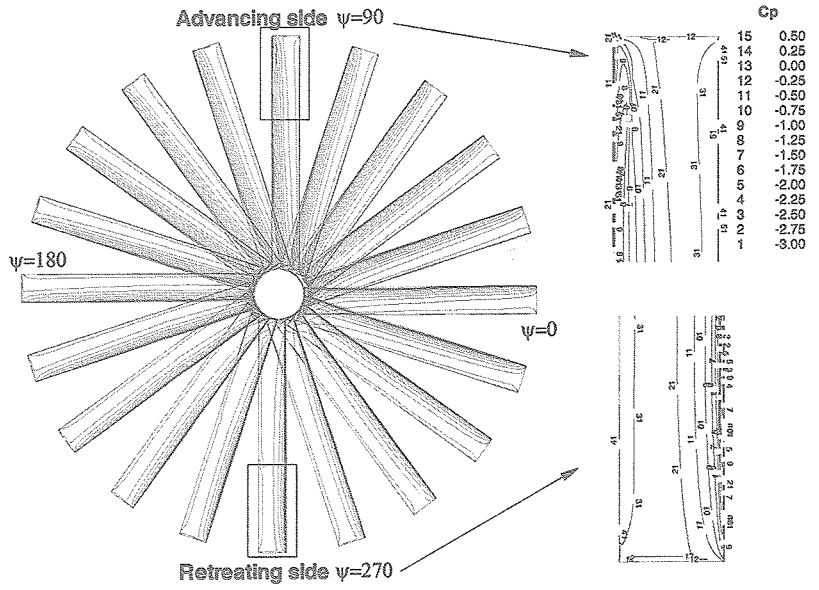

Upper surface

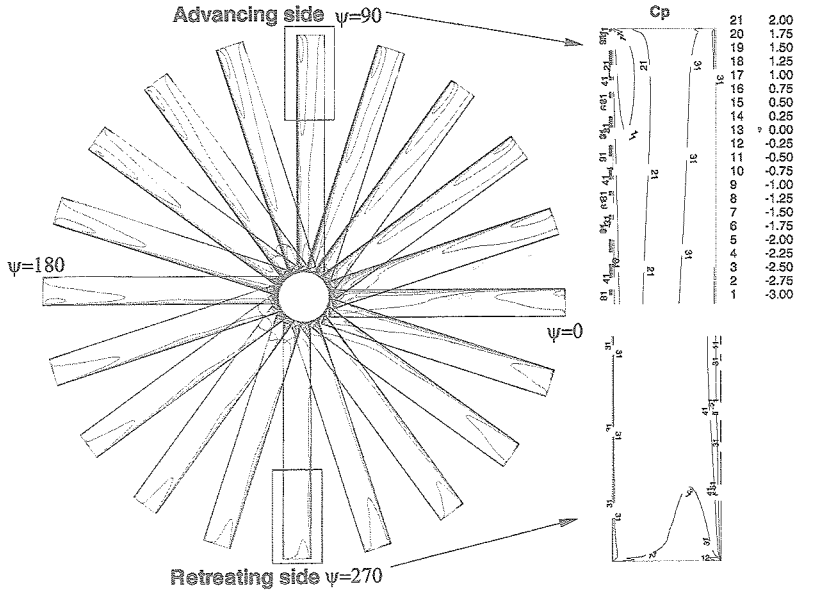

Lower surface

(a) no jet

Figure 3.14 Pressure coefficient distribution according to azimuth angles

forces along the spanwise direction for various jet conditions at azimuth angle of 0 degree and 306 degree. The results showed that any kinds of jet blowing from the rotor tip caused the increased lift coefficient (C_l) distributions and lift forces near tip region, and these increase are thought to originate the phenomena so called the increased 'wing-span' by the jet blowing.

According to azimuth angles, each rotor blade experiences unsteady pressure history, which has a sudden change when blade-vortex interaction happens. After applying aeroacoustic code based on Ffowcs-Williams and Hawkings formulation, we can get sound pressure history for one revolution of rotor. Figure 3.19 shows the comparison of sound pressure level (SPL) histories for one revolution of rotor blade according to the jet conditions. Compared to the results of single

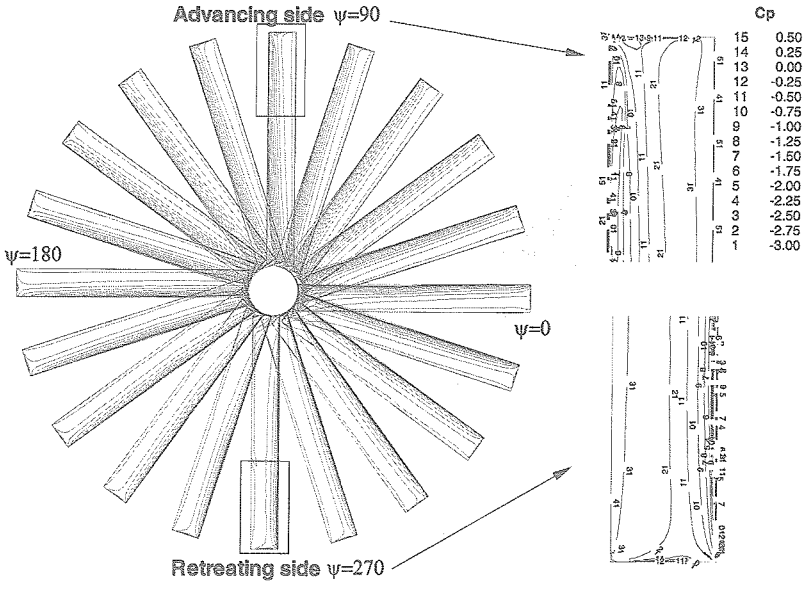

Upper surface

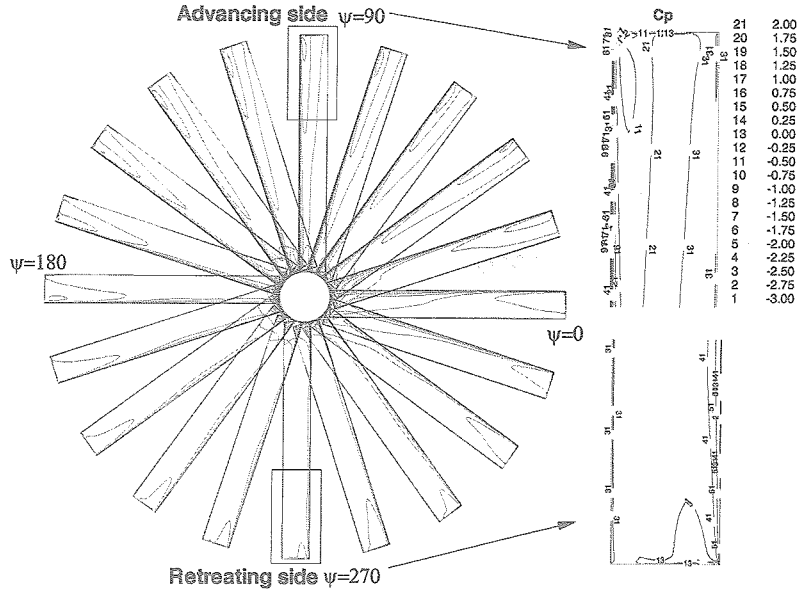

Lower surface

(b) wide and fast jet

Figure 3.14 ((continued))

fixed blade calculation, the solutions of different jet condition show not so much difference with each other. The reason of small effect of jet blowing can be thought of a numerical dissipation in the inner background grid, which is sparse to project the tip vortex core correctly. The numerical dissipation causes this result in spite of using higher accuracy numerical scheme.

Maximum BVI noise peak, which is shown in the positive peak value, is reduced when jet blowing is applied at rotor tip with any kinds of jet conditions. Even the other BVI noise in the negative peak value increased owing to jet blowing, the method to use jet blowing is effective to reduce the peak BVI noise, which is more critical to human's hearing.

As shown in Table 3.2 of sound pressure level, when converted into sound level, the maximum decrease in

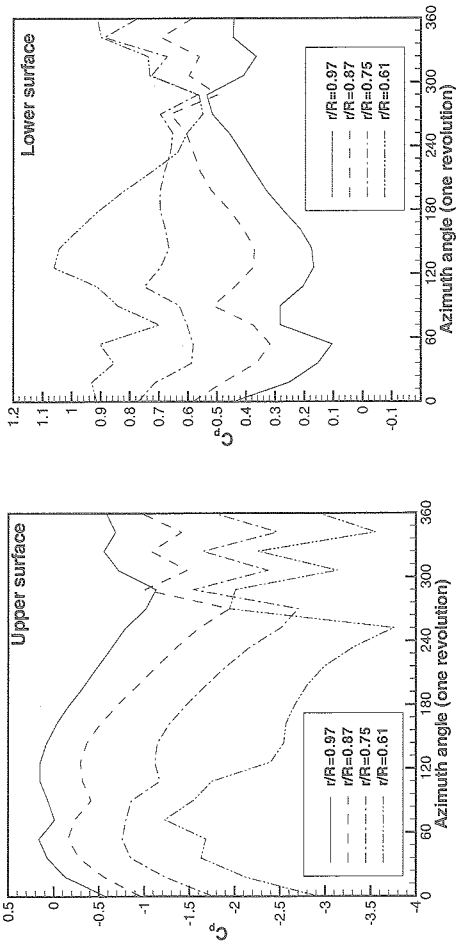

(a) nojet

(b) normal jet

Figure 3.15 Computed pressure coefficient (C_p) histories on blade surface

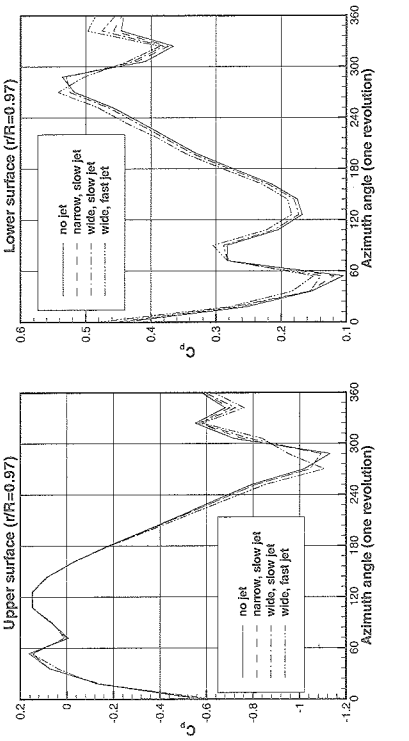

Figure 3.16 Comparison of pressure coefficient (C_p) according to various jet conditions for one revolution at one position near leading edge on upper and lower blade surface

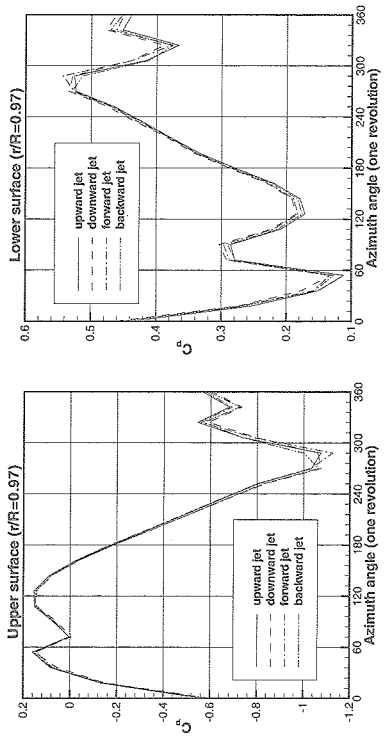

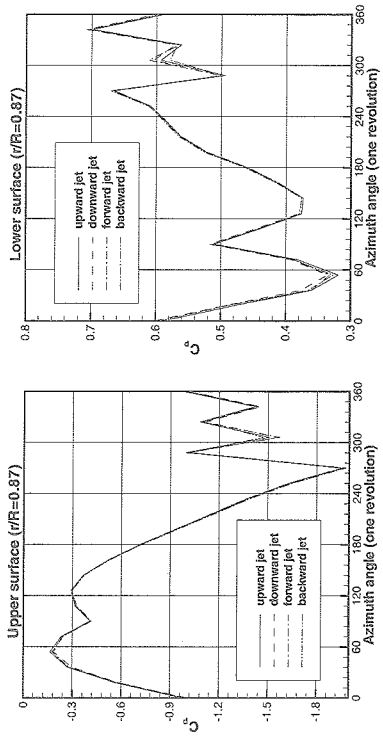

Figure 3.16 ((continued))

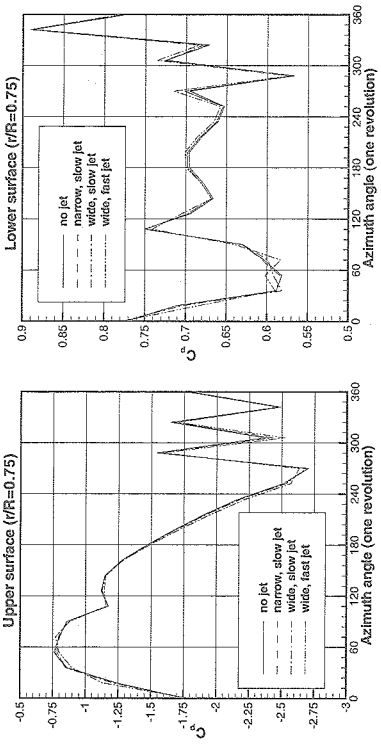

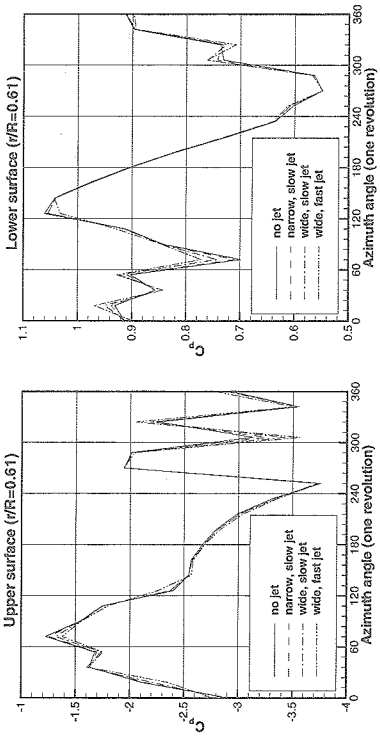

Figure 3.16 ((continued))

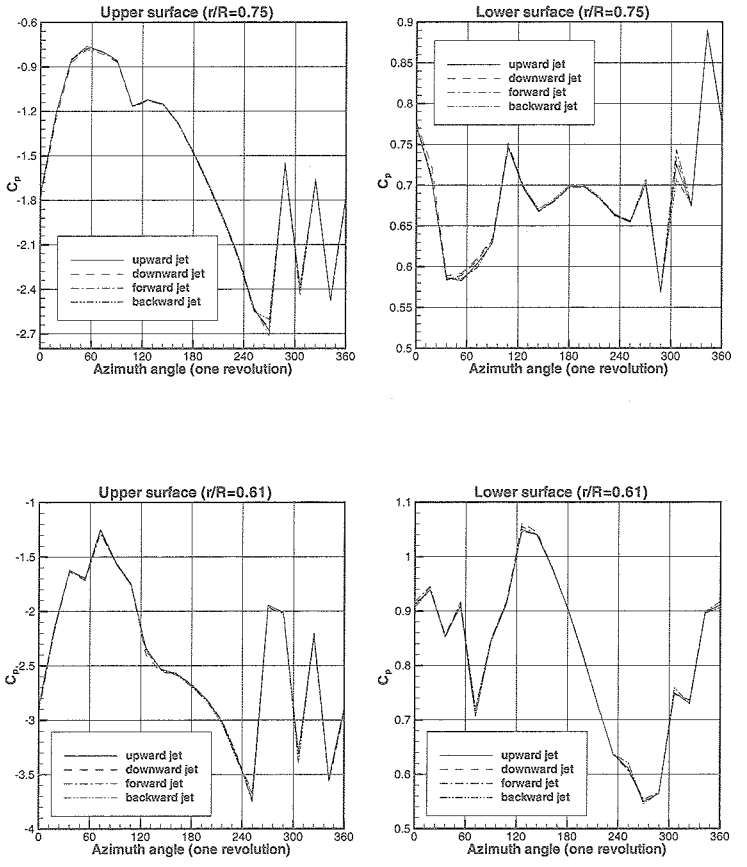

Figure 3.16 ((continued))

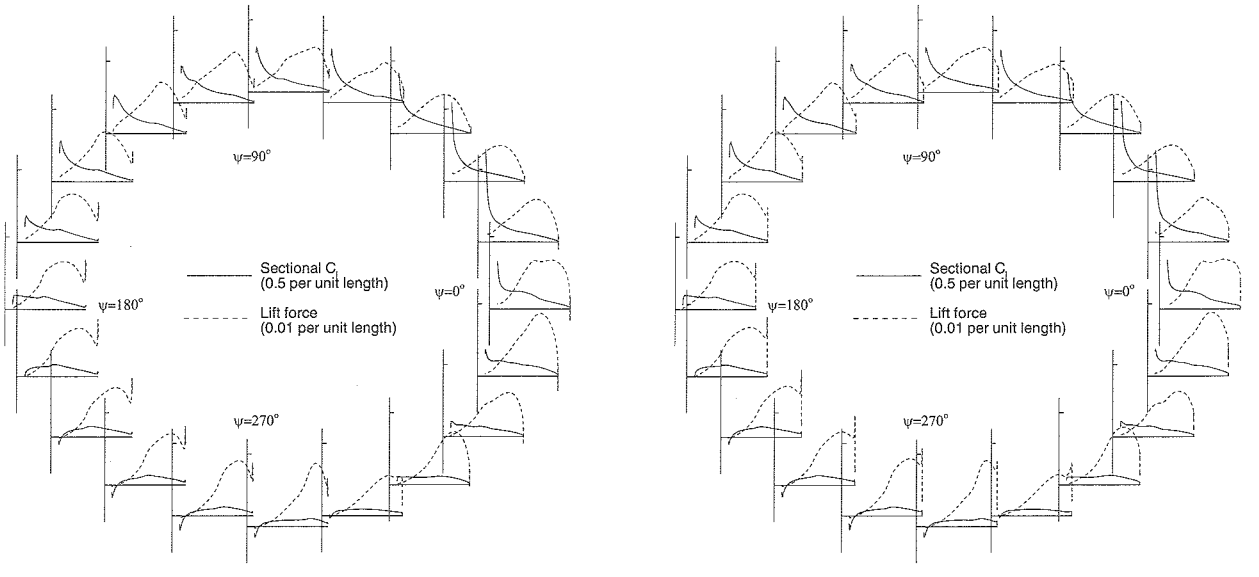

(a) no jet *(b) fast, wide jet*

Figure 3.17 Sectional lift coefficient (C_l) distributions along the spanwise direction for azimuth angle

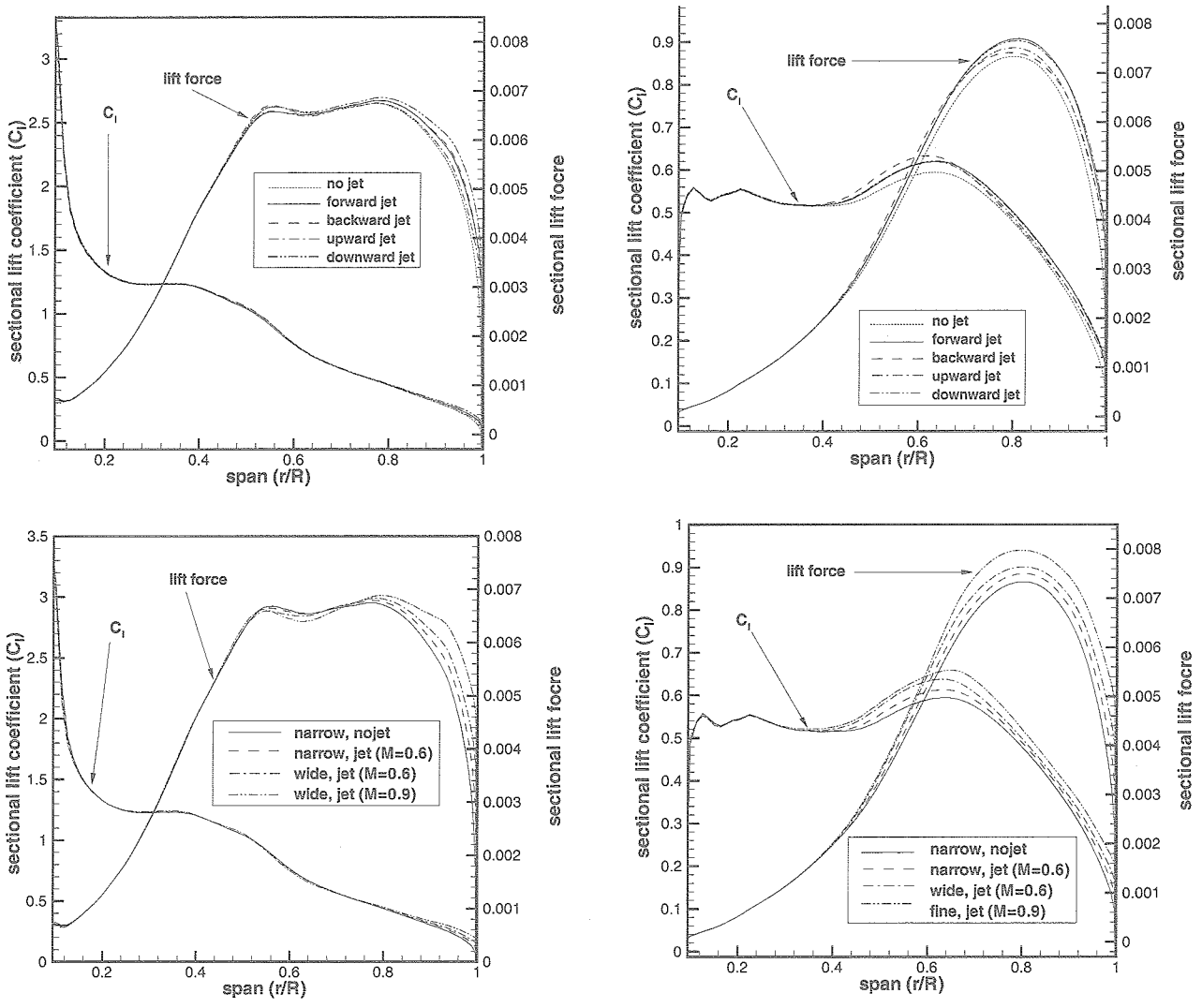

(a) $\psi = 0^o$ *(b)* $\psi = 306^o$

Figure 3.18 Comparison of sectional lift coefficient (C_l) distributions and lift forces along the spanwise direction for various jet conditions

Table 3.2 Comparison of BVI noise reductions for several cases

	SP (W/m^2)	Noise (dB)	difference (dB)
No Jet	18.62	119.38	—
Normal Jet (narrow, $M_j = 0.6$)	18.60	119.36	0.02
Normal Jet (wide, $M_j = 0.6$)	16.35	118.25	1.13
Normal Jet (wide, $M_j = 0.9$)	13.88	116.83	**2.55**
Forward Jet ($M_j = 0.6$)	17.87	119.02	0.36
Backward Jet ($M_j = 0.6$)	17.73	118.95	0.43
Upward Jet ($M_j = 0.6$)	18.03	119.10	0.28
Downward Jet ($M_j = 0.6$)	18.45	119.30	0.08

BVI noise is 2.55 dB for the wide and fast jet blowing.

From the results with overlapped grid system above, the effect of jet blowing direction is not so big to change the BVI noise, compared with the big difference as results with fixed blade. The reason is supposed to be the periodic alternation of flow condition of rotor owing to rotor rotation during forward flight.

These aeroacoustic results demonstrate the capability of our code to predict the BVI noise. However, inaccuracy of miss-distance between vortex core and rotor blade causes some disagreements of intensity and location of BVI. The strong downwash induced by the over-prediction of thrust causes descend of tip vortices that strongly affect BVI property. Consideration of blade elasticity and correction of control input (e.g. collective

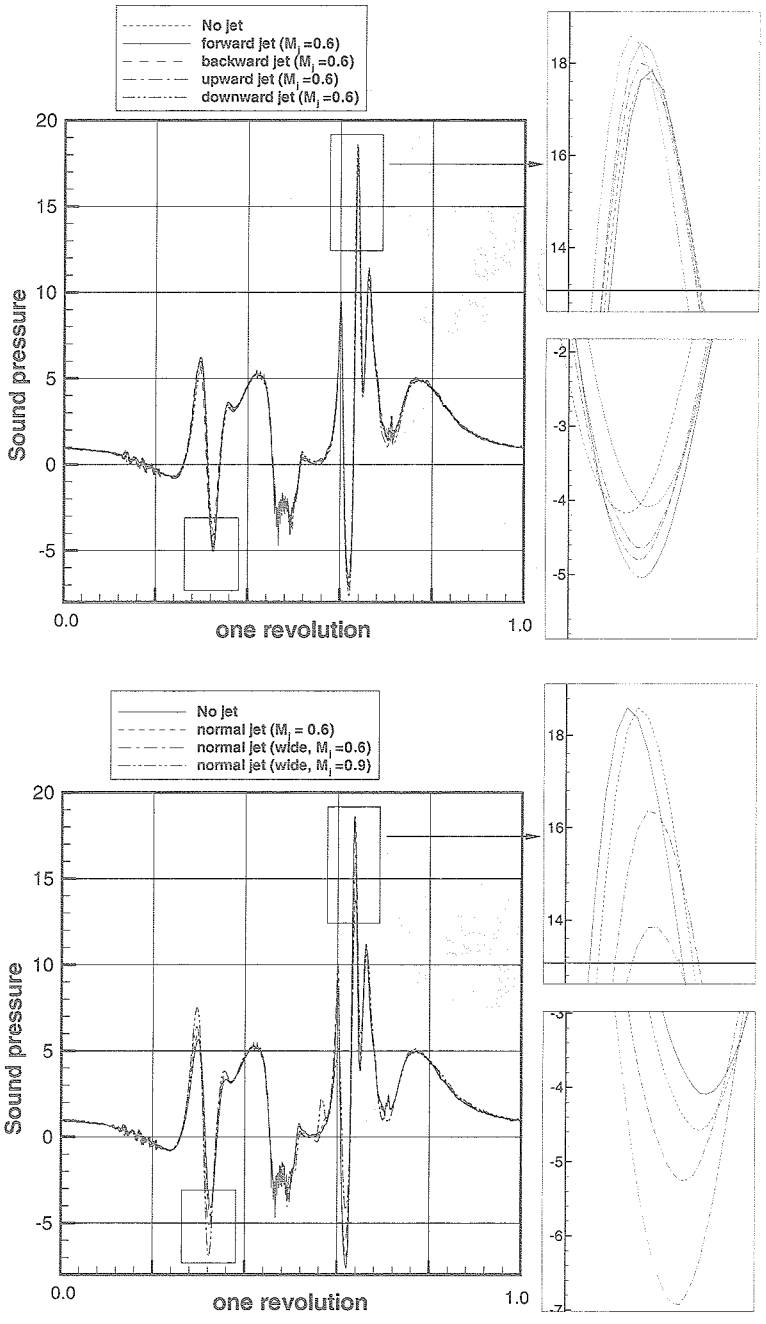

Figure 3.19 Comparison of sound pressure level (SPL) between cases with overlapped grid system

and cyclic pitch angles) should be made for the improvement of the prediction. Improvements in CFD computation, especially in the estimation of tip vortex positions, will be required to obtain more accurate noise prediction. It is necessary to study more about the effect of discrete jet blowing according to flight condition and rotor movement.

3.3 Study on the grid dependency

The predictions of Blade-Vortex Interaction (BVI) noise with fine grid system are performed using a combined method of an unsteady Euler code with an aeroacoustic code based on Ffowcs-Williams and Hawkings formulation. Two different inner background grids (fine and coarse) are constructed for testing the grid dependency. A blade grid and outer background grid in moving overlapped grid system are used the same as

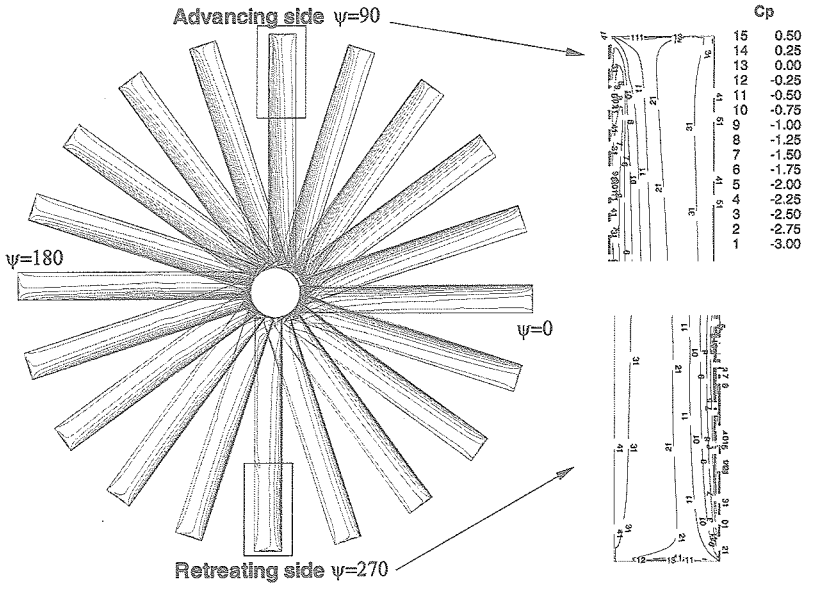

Upper surface

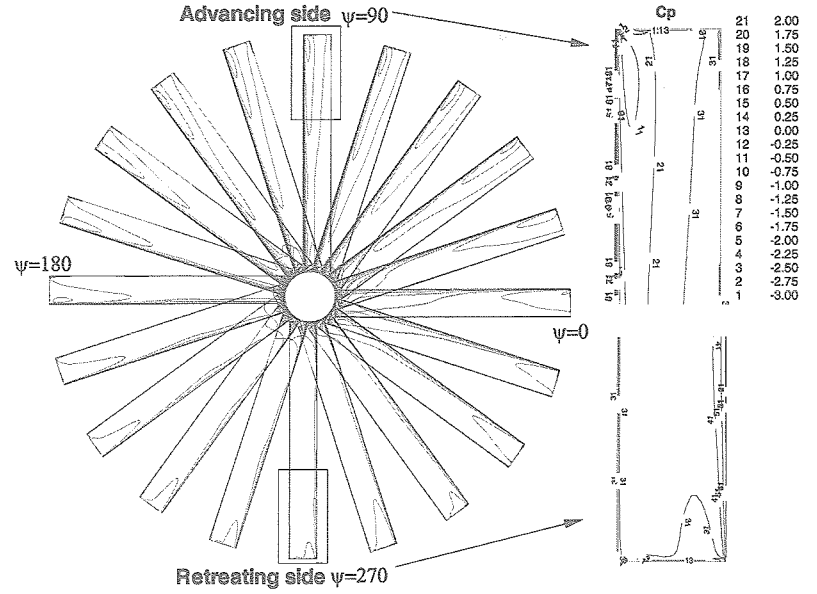

Lower surface

(a) fine grid without jet

Figure 3.20 Pressure coefficient distribution according to azimuth angles for upper and lower blade surface

the previous calculation, and inner background grid is rebuilt using nearly 1.8 times more grids in each direction than the previous one. BVI of helicopter with two OLS-airfoil blades in forward/ descending flight condition are simulated with and without jet blowing. As mentioned in the numbers of grid points for each grid system of Table 2.1, the grid spacing of the inner background grid corresponds to 0.11c (fine) and 0.19c (coarse), where c is the chord length.

Figure 3.20 shows the pressure coefficient distribution according to azimuth angles for upper and lower blade surface using fine grid system in inner background grid. The pressure coefficients show the similar patterns globally with those of coarse grid system, but the fine grid system calculated more specified pressure field near the tip region at both advancing and retreating sides. It

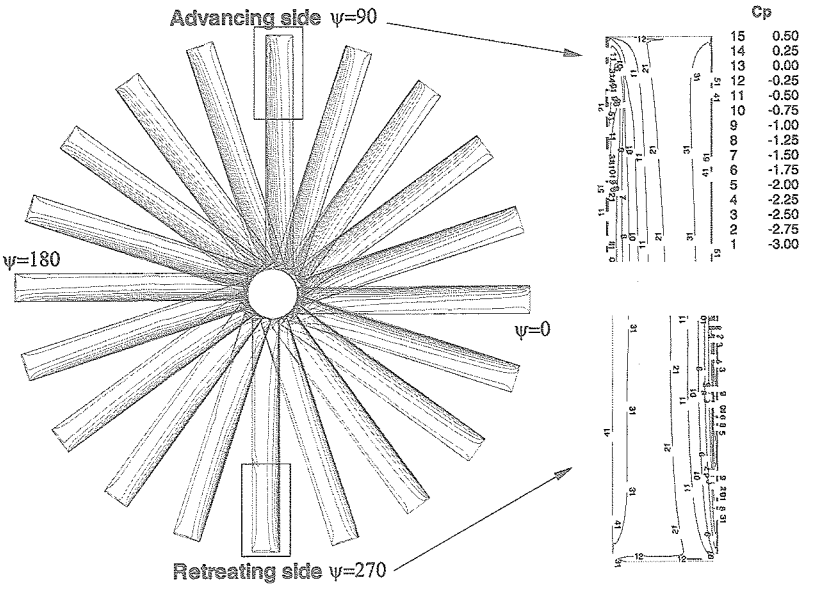

Upper surface

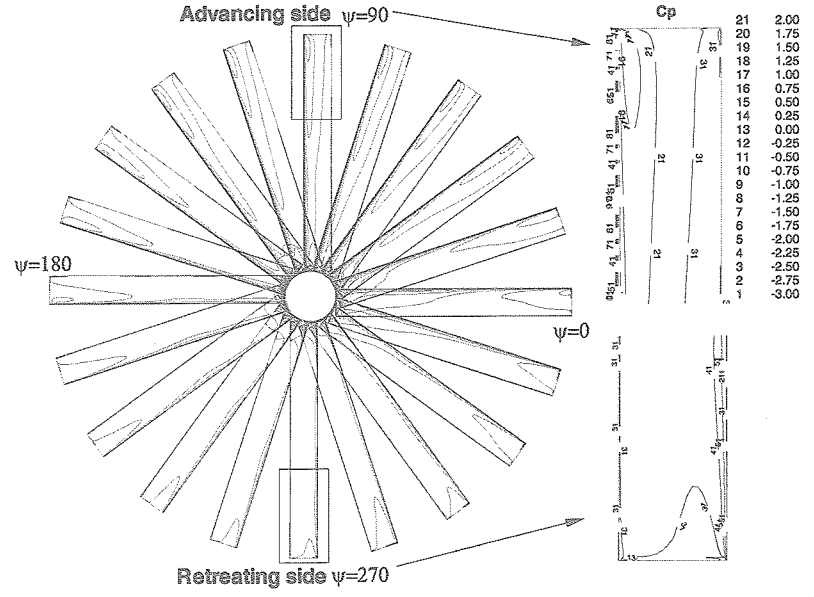

Lower surface

(b) fine grid with normal jet

Figure 3.20 ((continued))

means that even the fine grid system is mainly related to the inner background system, the flow field in blade grid system is affected from changing boundary interpolation.

Figure 3.21 shows the computed pressure coefficient (C_p) histories on upper and lower blade surfaces, and Figure 3.22 shows the comparison of pressure coefficient (C_p) histories for one revolution at one position near leading edge on upper and lower blade surface using fine grid system. With these figures, we can show the change of global quantities according to the grid system and jet condition. The greatest difference occurs at the retreating side (from 270° to 360°) in the tip region (r/R = 97% and 87%).

Figure 3.23 shows the lift coefficient distributions and lift forces along the spanwise direction for azimuth angle with and without jet conditions. Figure 3.24 shows the

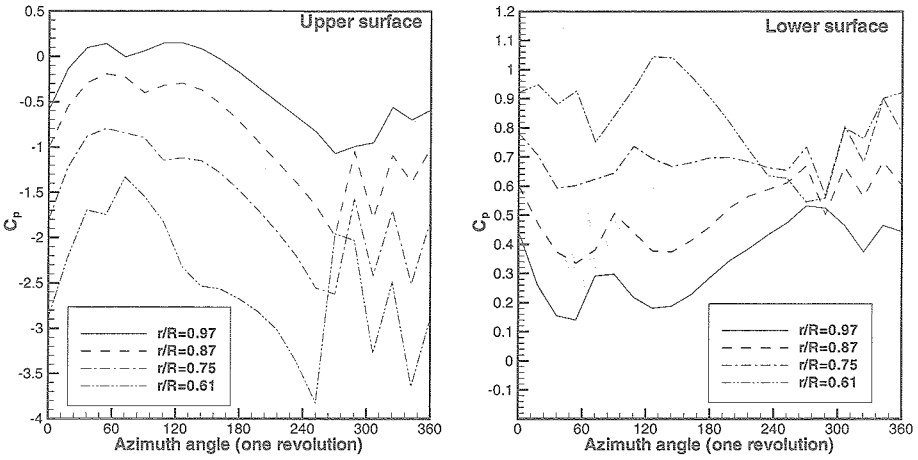

(a) fine grid without jet

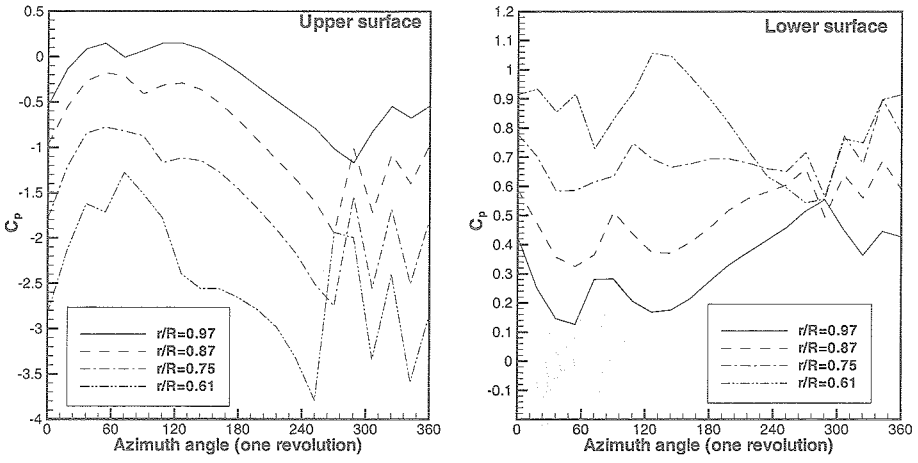

(b) fine grid with normal jet

Figure 3.21 Pressure coefficient (C_p) histories on upper and lower blade surfaces

comparison of lift coefficient distributions and lift forces along the spanwise direction for both grid systems and jet conditions at azimuth angle of 0 degree and 306 degree, where differences are critical according to grid systems.

In Figure 3.25, tip vortices are visualized by the iso-surface of vorticity magnitude in the inner background grid at top view for coarse and fine grid systems with/without jet condition. Even the similar image in the iso-surface is observed between both coarse and fine grid results, a distinct difference in the iso-surface exists. For both coarse and find grid systems, the tip vortex generated from two blades in forward and descending flight moves slightly upward, but still remains near the rotation plane (or rotor disk), which makes blade vortex interaction. Compared to the values from coarse grid, the vorticity from fine grid are shown to keep its strength longer, which is displayed by the fact that vortex last more rotor revolutions. Also the effect of jet blowing is clearly seen when using the fine grid system.

Figure 3.26 also takes the different point of view for contours of vorticity magnitude in the cross section parallel to the flow direction ($r/R = 0.8$, retreating side). From these results, it is found that the coarse grid calculation captures only weak tip vortices. From this contour, we can see that the vortex generated from the preceding blade pass through the following blade. The tip vortex of fine grid system shows not only more clear and concentrated vortex but also stronger vorticity magnitude.

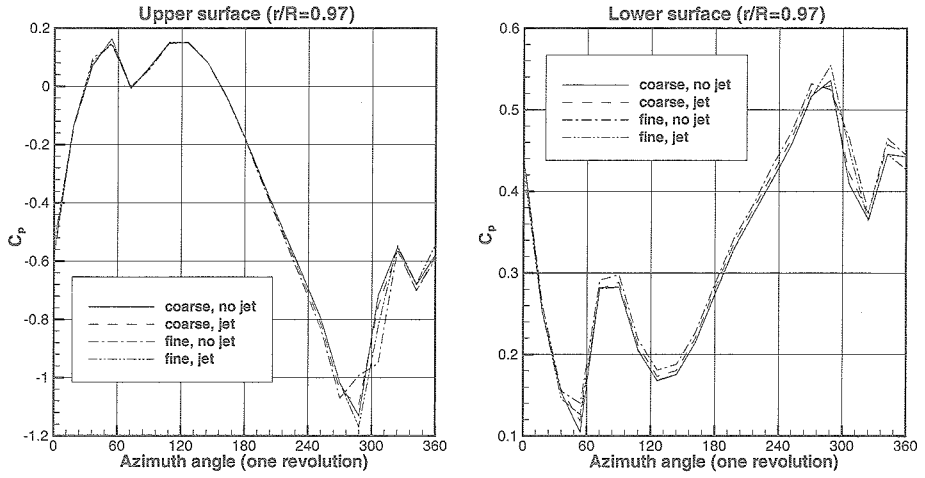

(a) r/R = 0.97

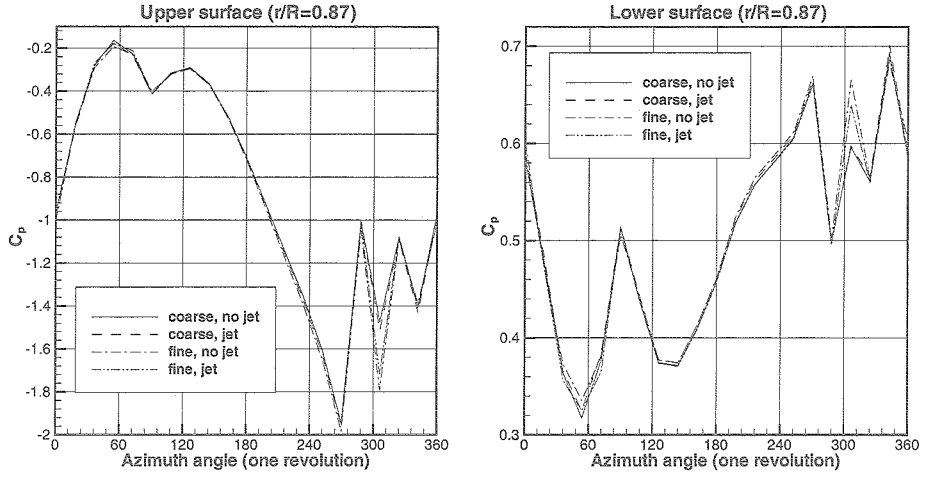

(b) r/R = 0.87

Figure 3.22 Comparison of pressure coefficient (C_p) histories for one revolution at one position near leading edge on upper and lower blade surface

There are two reasons for these differences between coarse and fine grid calculation. The first and most important reason is a numerical dissipation in the inner background grid. While tip vortices in the fine grid keep their strength, those in the coarse grid are dissipated immediately. The numerical dissipation causes this result in spite of using higher accuracy numerical scheme. The second reason is a loss of vorticity strength at the interpolation of flow data between blade grid and inner background grid. The loss is shown in the most upstream region where the blade grid system is located. The vorticity strength in the coarse grid is weaker than that of the fine grid, though the influence of numerical dissipation is negligible in this region because the tip vortex is just projected to the inner background grid. This vortex strength loss is caused by the lack of resolution of the coarse inner background grid. The grid spacing, 0.19c, of the coarse inner background grid is too sparse to project the tip vortex core correctly, which is generally 0.2c in diameter.

Figure 3.27 shows the comparison of sound pressure level (SPL) histories for both coarse and fine grid system with and without jet conditions. At the maximum peak position (A), the values of fine grid system shows the sharper peak in sound pressure level distribution than those of coarse grid. Considering the results of comparison of computed sound pressure level with that of experiment, the calculation with fine grid system

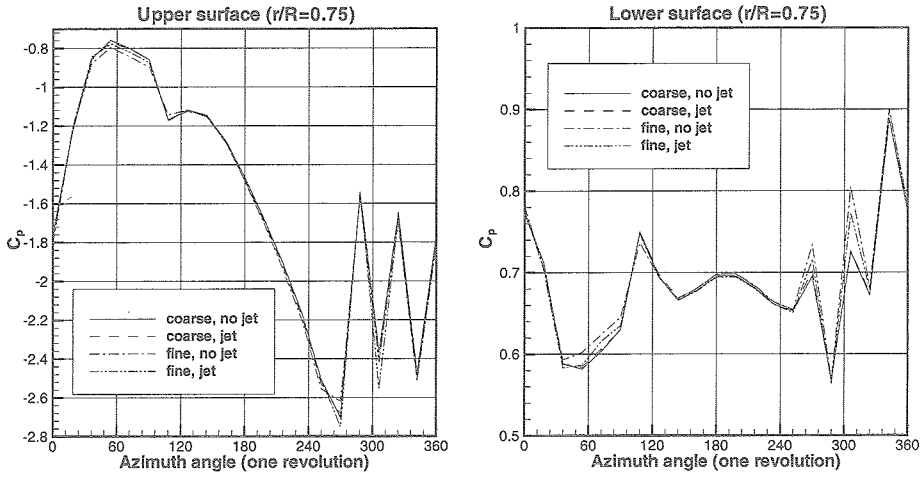

(c) r/R = 0.75

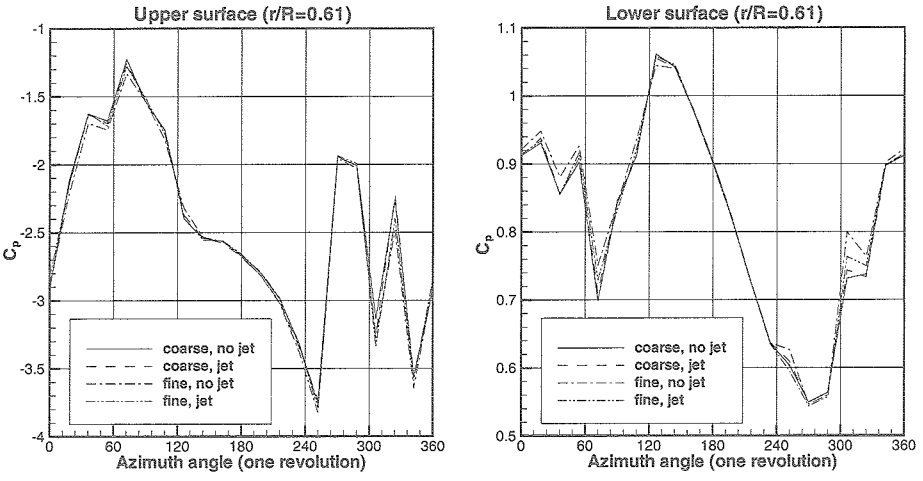

(d) r/R = 0.61

Figure 3.22 ((continued))

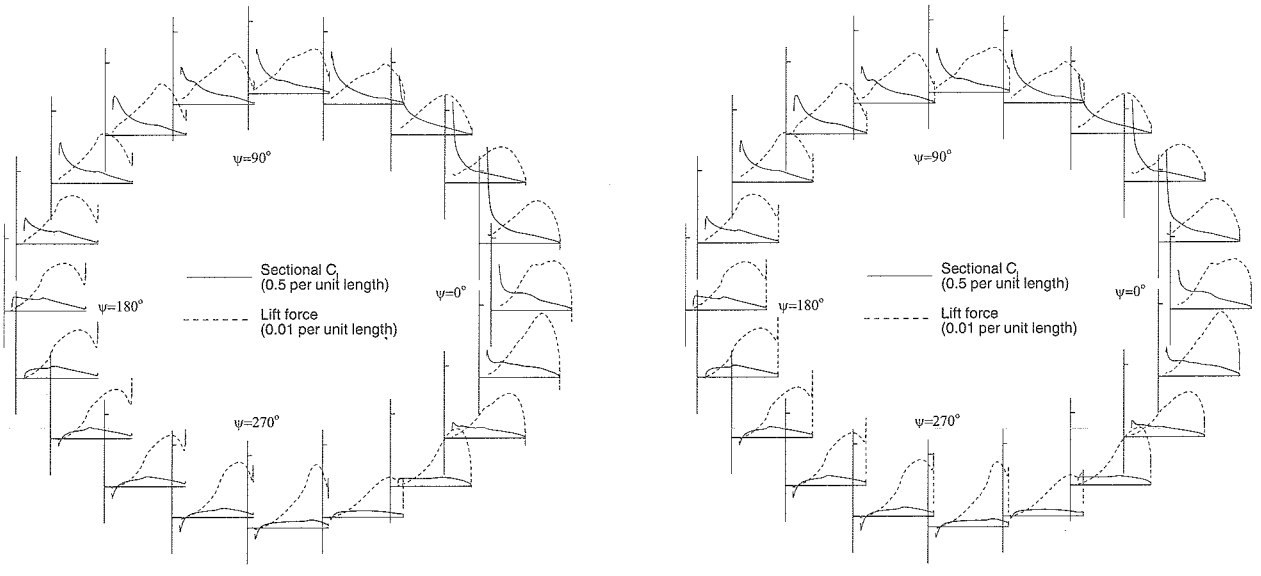

(a) fine grid without jet *(b) fine grid with normal jet*

Figure 3.23 Lift coefficient distributions and lift forces along the spanwise direction for azimuth angle

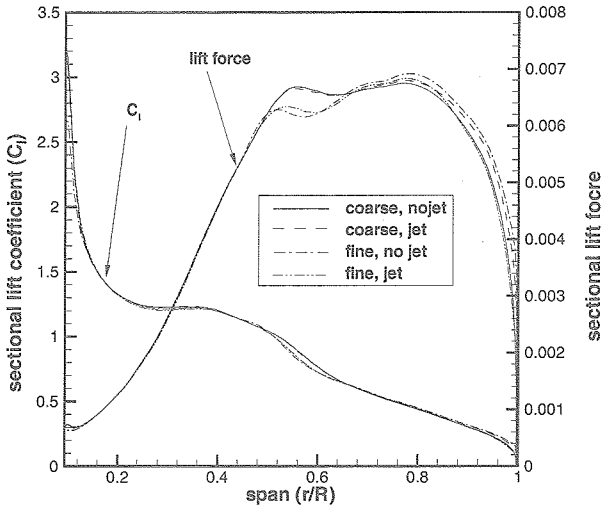

(a) $\psi = 0^o$

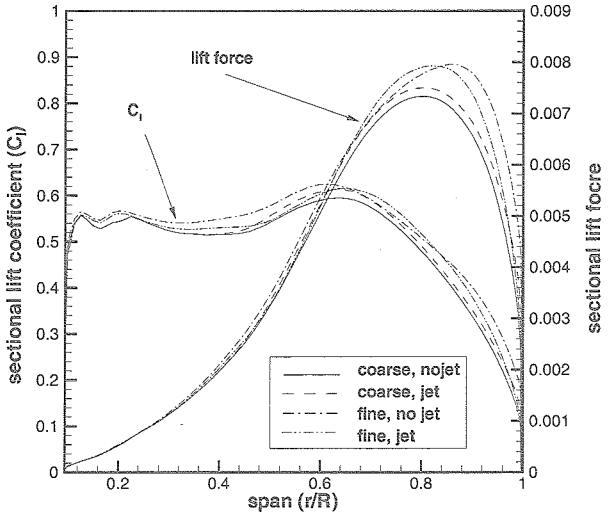

(b) $\psi = 306^o$

Figure 3.24 Comparison of lift coefficient distributions and lift forces along the spanwise direction for both grid systems and jet conditions

(a) coarse grid without jet

(b) fine grid without jet

Figure 3.25 Iso-surface of vorticity at top view for coarse and fine grid systems

approaches the experimental results in the way of larger peak values when blade vortex interaction happens, and it means that fine grid system should be used to get the more accurate solution of blade vortex interaction. And from the difference of sound pressure level between the cases with/without jet blowing, the fine grid system show more distinct decrease on account of the jet effect. It ascertains the conclusion of the previous chapter that jet blowing method can reduce the blade vortex interaction noise.

4. SUMMARY AND CONCLUSIONS

As one of the active control method to reduce Blade-Vortex Interaction (BVI) noise of helicopter rotor, the effects of lateral wing-tip blowing are analyzed for the generation and behavior of tip vortical flow from rotary two blades. Comprehensive numerical investigations on the tip vortical characteristics of fixed/rotary wing are performed for various conditions to get the following conclusions. The predictions of blade vortex interaction noise are performed using a combined method of an unsteady Euler code with an aeroacoustic code based on Ffowcs-Williams and Hawkings formulation. A moving overlapped grid system with three types of grids including blade grid, inner and outer background grid is used to simulate BVI of helicopter with two OLS-airfoil blades in forward/ descending flight condition.

(c) coarse grid with normal jet

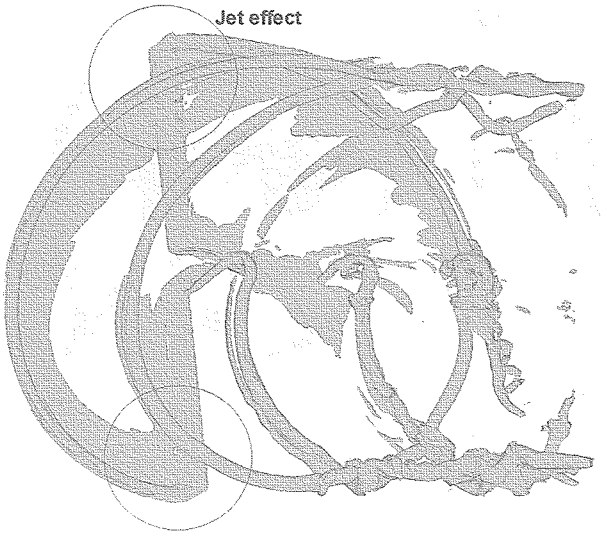

(d) fine grid with normal jet

Figure 3.25 ((continued))

(1) The calculated sound pressures of test cases are compared with experimental results, and showed good agreements in capturing the BVI noise peak. It means that this unsteady flow solver has the ability to simulate the BVI phenomena and BVI noise analysis can be successfully predicted when combined with aeroacoustic code.

(2) The jet blowing plays a positive role to reduce BVI noise in both ways: at first, by increasing the core size to produce less pressure gradient during BVI, and at second, by pushing the vortex center upward to increase miss-distance during BVI.

Table 3.3 Comparison of BVI noise reductions for several cases using fine grid system

	SP (W/m^2)	Noise (dB)	difference (dB)
No Jet	18.62	119.38	—
Normal Jet	18.60	119.36	0.02
Fine, No Jet	18.97	119.54	—
Fine, Normal Jet	18.49	119.31	0.23

(3) The effect of lateral blowing at tip to reduce BVI noise is examined using various jet blowing conditions including jet speed, jet slit area and injecting direction, and most of jet blowing can reduce the BVI peak noise more or less. Maximum BVI noise peak in sound pressure level is reduced for some jet condition at rotor tip, and when converted into sound level, the maximum decrease in BVI noise is 2.55 dB for the case with wide and fast jet blowing.

(4) The solution of fine grid showed more distinct peak of blade vortex interaction noise in sound pressure level. The minor difference between the cases with and without jet revealed more clearly in the solution of fine grid system than that of coarse one. The reason is a numerical dissipation in the inner background grid, which is most important to keep the accuracy of tip vortex calculation. The second reason is a loss of vorticity strength at the interpolation of flow data between blade grid and inner background grid.

With these results above, the method to use jet blowing can be effective way to reduce the peak noise in the helicopter BVI phenomena. The BVI noise can be solved well enough to check the global characteristics using coarse grid system, while fine grid system is suggested in order to obtain more accurate results of jet effect.

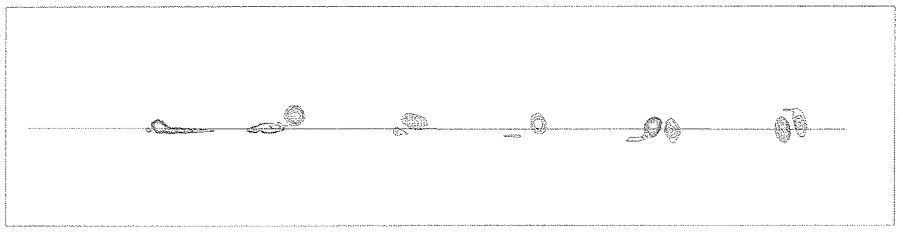

(a) coarse grid

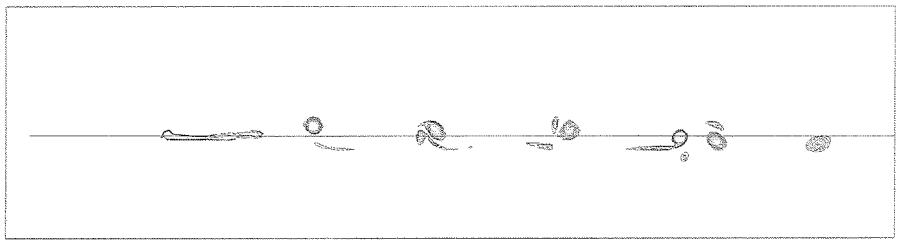

(b) fine grid

Figure 3.26 Vorticity contour on the spanwise intersection

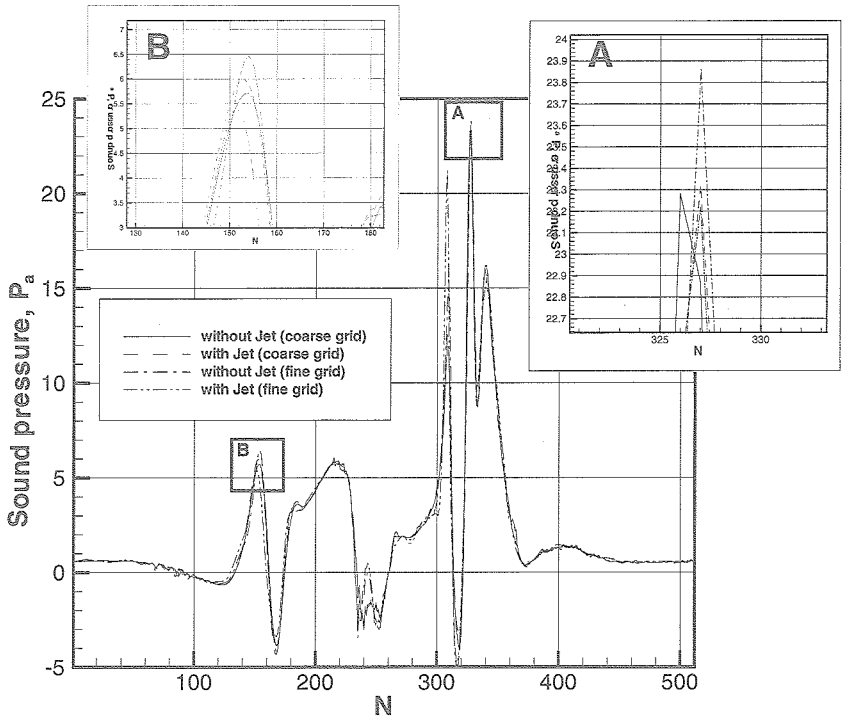

Figure 3.27 Comparison of sound pressure level (SPL) histories for both coarse and fine grid system with and without jet conditions

REFERENCES

[1] Lee, S. and Bershader, D., *Head-on parallel blade-vortex interaction*, AIAA Journal, Vol.32, No.1, pp.16–22, 1994

[2] Schmitz, F. H. and Yu, Y. H., *Helicopter impulsive noise: theoretical and experimental status*, Journal of Sound and Vibration, 109(3), pp.361–422, 1986

[3] Martin, R.M. and Cornor, A.B., *Wind-tunnel acoustic results of two rotor models with several designs*, NASA-TM 87698, 1986

[4] Sirinivasan, G. R., McCroskey, W. J. and Kutler, P., *Numerical Simulation of a Vortex with Stationary Airfoil in Transonic Flow*, AIAA-84-0254, 1984

[5] George, A. R. nd Chang, S.-B., *Flow Field and Acoustics of Two-Dimensional Transonic Blade-Vortex Interactions*, AIAA-84-2309, 1984

[6] Tung, C., Yu, Y. H., and Low, S. L., *Aerodynamic aspects of blade-vortex-interaction(BVI)*, AIAA Paper 96–2010, 1996

[7] Matthewson, C.S., Vakili, A.D. and Gowanlock, D.K., *Adaptive control of wingtip vortex flows*, AIAA, 98–0318, 1998

[8] Vakili, A.D., Matthewson, C.S. and Gowanlock, D.K., *Control of helicopter blade tip vortex*, AIAA, 98–2240, 1998

[9] Saito, S., Aoyama, T., Ochi, A., Kondo, N. and Yamaguchi, A., *Impulsive noise calculation using moving overapped grid method/ Kirchhoff method*, 25th European Rotorcraft Forum, B2: 1–11, 1999

[10] Hassan, A.A., Straub, F.K. and Charles, B.D., *Effects of surface blowing/suction on the aerodynamics of helicopter rotor blade-vortex interaction (BVI) - A numerical simulation*, J. of American Helicopter society, Vol.42: 182–194, 1997

[11] Tung, C., Caradonna, F. X. and Johnson, W., *The prediction of transonic flows on advancing rotors*, Journal of American Helicopter Society, Vol. 31, pp.4–9, 1986

[12] Boniface, J. C. and Pahlke, K., *Calculations of multibladed rotors in forward flight using 3D Euler methods of DLR and ONERA*, 22nd European Rotorcraft Forum, 1996

[13] Boniface, J. C., Mialon, B., and Sides, J., *Numerical simulation of unsteady Euler flows around multibladed rotors in forward flight using a moving grid approach*, AHS 51st Annual Forum, 1995

[14] Ochi, A., Shima, E., Aoyama, T., Saito, S. and Yamakawa, E., *BVI noise prediction by moving overlapped grid method*, AHS 55th Annual Forum, 1999

[15] Tadghighi, H., Hassa, A., and Charles, B., *Prediction of blade-vortex interaction noise using airloads generated by a finite-difference technique*, AHS 46th Annual Forum, 1990

[16] Yu, Y.H., Tung, C. and Gallman, J., *Aerodynamics and acoustics of rotor blade-vortex interaction*, Journal of Aircraft, Vol.32, No.5, pp.970–977, 1995

[17] Caradonna, F. et al., *A review of methods for the prediction of BVI noise*, AHS technical specialist' meeting for rotorcraft acoustics and aerodynamics, 1997

[18] Aoyama, T., Kawachi, K., Saito, S. and Kamio, J. *Unsteady analysis of transonic helicopter rotor noise*, 19th European Rotorcraft Forum, 1993

[19] Aoyama, T., Kondo, N., Aoki, M., Nakamura, H. and Saito, S. *Calculation of rotor blade-vortex interaction noise using parallel super computer*, 22nd European Rotorcraft Forum, 1996

[20] Jacklin, S.A. and Nguyen, K. Q., *Full-scale wind tunnel test of a helicopter individual blade control system*, 50th Annual Forun of the Americal Helicopter Society, 1994

[21] Splettstoesser, W., R. Kube, W. Wagner, et al., *Key results from a higher harmonic control aeroacoustics rotor test (HART)*, J. of American Helicopter society Vol.42, No.1 pp.58–78, 1998

[22] Hassan, A. A., Charles, B. D., Tadgahighi, H. and Sankar, L. N., *Blade-mounted trailing edge flap control for BVI noise reduction*, NASA Contractor Report 4426, 1992

[23] Araki, R., Obayashi, S., Nakahashi, K., Tsukahara, T., Obukata, M., and Nakadate, M., *A numerical method for blade vortex using vortex confinement*

[24] Ota, T., Hashiguchi, Y., Tsukahara, T., Obukata, M., and Nakadate, M., *BVI noise reduction with Canard blade tip* (1st Report)

[25] Lee, C.S., Tavella, D., Wood, N.J. and Roberts, L., *Flow structure and scaling laws in lateral tip blowing*, AIAA Journal, Vol.27, No.8, Paper No.86–1810, 1988

[26] Lee, C.S., Tavella, D., Wood, N.J. and Roberts, L., *Lift modulation with lateral wing-tip blowing*, Journal of Aircraft, Vol.25, No.4, 1988

[27] Lee, C.S., Tavella, D., Wood, N.J. and Roberts, L., *Influence of wing-tip configuration on lateral bowing efficiency*, AIAA 24th Aerospace Science Meeting

[28] Wu, J.M., Vakili, A.D. and Chen, Z. L., *Wing tip jets aerodynamic performance*, Proceedings of the 13th Congress of the International Council of the Aeronautical Science, ICAS 82-5.6.3, 1982

[29] Wu, J.M., Vakili, A.D. and Gilliam, F.T., *Aerodynamic interaction of wingtip flow with discrete wingtip jets*, AIAA Paper 84-2206, 1984

[30] Wu, J.M., Vakili, A.D. and Mo, J.D., *Investigation of phenomena of discrete wingtip jets*, UTSI Report 88–06

[31] Wu, J.M., Vakili, A.D. Chen, Z.L., and Gilliam, F.T., *Investigation of the effect of discrete wingtip jets*, AIAA Paper 83–0546, 1983

[32] Gowanlock, D.K. and Matthewson, C.S., *Control of rotor tip vortices*, AIAA, 99–0012, 1999

[33] Mineck, R.E., *Study of Potential Aerodynamic Benefits From Spanwise Blowing at Wingtip*, NASA Technical Paper 3515, 1995

[34] Tan, A., Hara, Y. and Shindo, S. *Reduction of BVI noise by blowing air from blade tip*, Japanese Aircraft Symposium, 35th: 73–76; 1997

[35] Yamada, L., *Numerical Analysis of Tip Vortex Generated by Helicopter Blade*, Dissertation of M.S., Science University of Tokyo, 1999

[36] Yang, C.M., Baek, J.H., Saito, S., Shirai, M., Suenaga, H, Yamada, R., Nishizawa, U., Tan, A. Kanehira, N., and Shindo, S., *Numerical and experimental investigations of tip vortex with lateral wing-tip blowing*, 26th European Rotorcraft Forum, 2000

[37] Caradonna, F.X. and Isom, M.P., *Subsonic and transonic potential flow over helicopter blades*, AIAA Journal, Vol.10, pp.1606–1612, 1972

[38] Strawn, R.C. and Caradonna, F.X., *Numerical modeling of rotor flows with a conservative form of the full-potential equation*, AIAA Paper 86–0079, 1986

[39] Mansour, N. N., *Numerical Simulation of the Tip Vortex Off a Low-Aspect Ratio Wing at Transonic Speed*, AIAA Journal, Vol.23, Aug., pp. 1143–1149, 1985

[40] Kaynak, U., Holst, T., Cantwell, B. J., and Sorenson, R. L., *Numerical Simulation of Transonic Seperated Flows over Low-Aspect Ratio Wings*, *Journal of Aircraft*, Vol.24, Aug., pp. 531–539, 1987

[41] Srinivasan, G. R., McCroskey, W., J., Baeder, J. D., and Edwards, T. A., *Numerical Simulation of Tip Vortices of Wings in Subsonic and Transonic Flows*, AIAA Journal, Vol.26, Oct., pp. 1153–1162, 1988

[42] Johnson, W., *Rotorcraft aerodynamics applications of comprehensive analysis*, Heli-Japan 98, Paper No.S5, Gifu, Japan, April 1998

[43] Ochi, A., Shima, E., Aoyama, T., and Saito, S., *A numerical simulation of flow around rotor blades using overlapped grid*, Proceedings of the 15th NAL Symposium on Aircraft Computational Aerodynamics (NAL SP-37), pp.211–216, Tokyo, Japan, Jul 1997

[44] Ochi, A., Aoyama, T., Saito, S., Shima, E. and Yamakawa, E., *Aerodynamic and Aeroacoustic Analysis of BVI by Moving Overlapped Grid Method*, 24th European Rotorcraft Forum, Paper No. AC04, 1998

[45] Roe, P.L., *Approximate Riemann solvers, parameter vectors, and differenece schemes*. Journal of Computational Physics, Vol.43: 357–372, 1981

[46] Bram van Leer, *Flux-Vector Splitting For The Euler Equations*, Lecture Notes on Physics, Vol. 170, pp. 507–512, 1982

[47] Katz, J. and Plotkin, A., *Low-Speed Aerodynamics - From Wing Theory to Panel Methods*, McGraw-Hill Inc., pp.331–342

[48] Chakravarthy, S. R., and Oscher, S., *A new class of high accuracy TVD schemes for hyperbolic conservation laws*, AIAA paper 85–0363, 1985

[49] Yamamoto, S. and Daiguji, H., *Higher-order-accurate upwind schemes for solving the compressible Euler and Navier-Stokes equations*, Journal of Computers & Fluids, 22, pp.259–270, 1993

[50] Shima, E. and Jounouchi, T., *Role of CFD in aeronautical engineering (No.14)–AUSM type upwind cchemes–*, Proceedings of the 14th NAL Symposium on Aircraft Computational Aerodynamics (NAL SP-34), pp.7–12, Tokyo, Japan,

Jul 1996

[51] Yamaguchi, A., *Study of helicopter rotor noise*, M.S. Thesis, Toukai university, 2000

[52] Lighthill, M. J., *Sound generated aerodynamics*, Proc. Roy. Soc. London, series A, Vol.267, No,1329, pp.147–182, 1962

[53] Farassat, F. and Brenter, K. S., *The uses and abuses of the acoustic analogy in helicopter rotor noise prediction*, AHS specialists' Meeting on Aerodynamics and Aeroacoustics, Arlington, Texas, 1987

[54] Brentner, K. S., Lyrintzis, A. S. and Koutsavdis, E. K., *A comparison of computational aeroacoustic prediction methods for transonic rotor noise*, American Helicopter Society 52nd Annual Forum, 1996

[55] Brentner, K. S., *Modeling aerodynamically generated sound: Recent advances in rotor noise prediction*, 38th AIAA Aerospace Science Meeting and Exhibit, Reno, Navada, AIAA paper 2000–0345, 2000

[56] Farassat, F. and Myers, M. K., *Aerodynamics via acoustics: Application of acoustic formulas for aerodynamic calculations*, AIAA 10th Aeroacoustics Conference, AIAA 86-1877, 1986

[57] Brentner, K. S., *Helicopter rotor noise prediction: Background, current status, and future direction*, Seminar in University Tennessee Space Institute, Chattanooga, Tennessee, 1997

[58] Boxwell, D.A., Schmitz, F.H., Splettstoesser, W.R. and Schults, K.J., *Helicopter model rotor-blade vortex interaction impulsive noise: scalability and parametric variations*, J. of American Helicopter society Vol.32, No.1 pp.3–12, 1987

[59] Heyson, H. H., *Linerized Theory of Wind-Tunnel Jet-Boundary Corrections and Ground Effect for VTOL-STOL Aircraft*

Acknowledgement

I would like to thanks to the assistances and advices from Akio Ochi and Natsuki Kondo in ATIC (Advanced Technology Institute of Commuter-helicopter, Ltd.).

Also this research work has been partially supported by Brain Korea 21 (BK21) program of Korea during author's staying in Japan from February to May in 2001.

Appendix

Experimental System in DNW

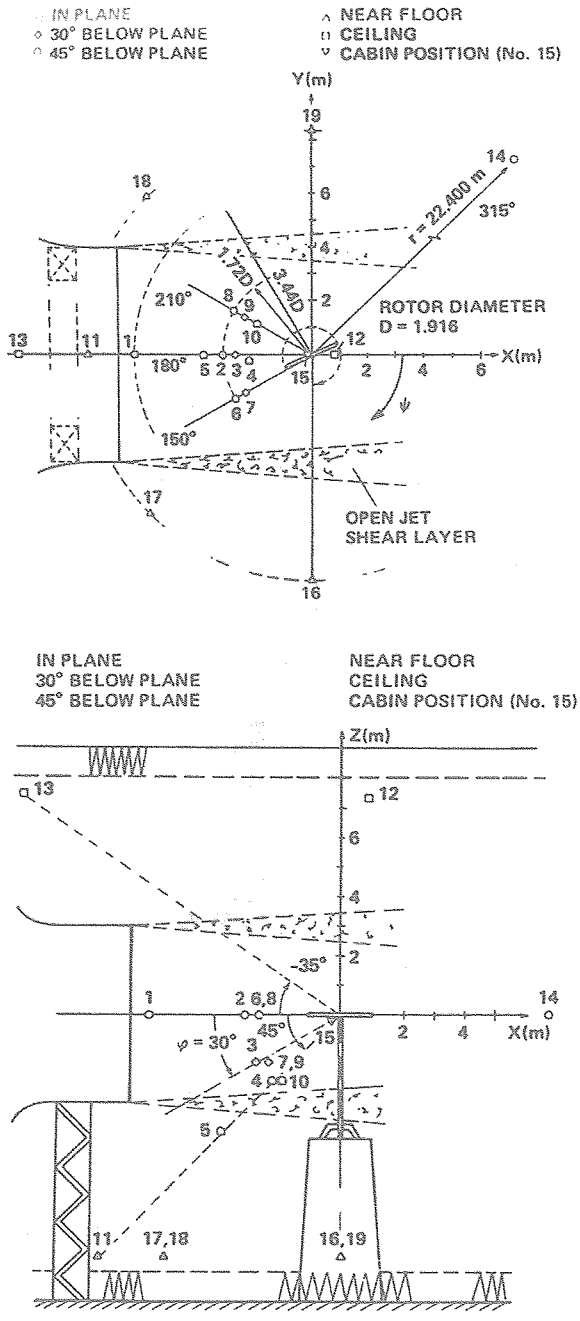

Ref. Boxwell, D.A., Schimitz, F.H., Splettstoesser, W.R. and Schults, K.J., "Helicopter model rotor-blade vortex interaction impulsive noise: scalability and parametric variations", Journal of American Helicopter Society, Vol.32, No.1, pp.3–12

JAXA Research and Development Report
(JAXA-RR-04-014E)

Date of Issue: Jan. 31, 2005

Edited and Published by:
Japan Aerospace Explortion Agency
7-44-1 Jindaiji-higashimachi, Chofu-shi,
Tokyo 182-8522 Japan

Printed by:
TOKYO PRESS Co., Ltd.
2-27-12 Sakuragawa, Itabashi-ku, Tokyo 174-0075 Japan

Japan Aerospace Exploration Agency